How Bacterial Vesicles Trigger Hearing Loss: The Role of Pyroptosis in Cochlear Damage

Xu Tong[a]， Junhong Zhang[b], Hao Zhao[c], Huiming Nong[b], Qianqian Yang[d], Yingxue Yuan[e], Jingyi Zhao[e], Xiru Zhang[e], Yanan Li[b], Zin Mie Mie Tun[f], Laurent A. Bekale[f*], Zhixin Cao[e*]

[a]Department of Otolaryngology-Head and Neck Surgery, Affiliated Qingdao Third People's Hospital, Qingdao University, Department of Otorhinolaryngology Head and Neck, Qingdao,266021,China
[b]Department of Otolaryngology-Head and Neck Surgery, Shandong Provincial Hospital Affiliated to Shandong First Medical University, Jinan 250021, Shandong, China
[c]Department of Otolaryngology, Head and Neck Surgery, People's Hospital, Peking University, Beijing 100871, China,
[d]Department of Pathology, the First Affiliated Hospital of Soochow University, Suzhou 215000, China
[e]Department of Pathology, Shandong Provincial Hospital Affiliated to Shandong First Medical University, Jinan 250021, Shandong, China
[f]Department of Otolaryngology, Head and Neck Surgery, Stanford University, 801 Welch Road, Stanford, CA 94305-5739, USA

*Corresponding authors: Laurent A. Bekale: bakale20@stanford.edu and Zhixin Cao: caozhixin12@126.com

ABSTRACT

Chronic suppurative otitis media (CSOM) is not just a bacterial infection of the middle ear but a leading cause of sensorineural hearing loss (SNHL). Yet, the mechanisms by which this disease leads to SNHL have remained elusive until now. Our study uncovers how *Pseudomonas aeruginosa* outer membrane vesicles (OMVs) directly damage cochlear hair cells. In both in vitro and in vivo models, OMVs were found to attack outer hair cells (OHCs) in the basal cochlea, which are responsible for high-frequency hearing and independent of macrophage activity. Beyond this damage, OMVs trigger intense inflammation, marked by increased pro-inflammatory M1 macrophages, which worsens the damage. OMVs also activate the NLRP3 inflammasome, driving inflammatory cell death through pyroptosis. RNA sequencing and proteomics confirmed this pathway, and treatment with the NLRP3 inhibitor MCC950 significantly reduced hearing loss in animal models. These findings reveal a new therapeutic target in the NLRP3 inflammasome, offering hope for innovative treatments to prevent hearing loss in CSOM patients.

KEYWORDS: Outer membrane vesicles (OMVs), Chronic suppurative otitis media, Sensorineural hearing loss, *Pseudomonas aeruginosa* OMVs, NLRP3 inflammasome activation,

Pyroptosis in cochlear hair cells.

Graphical abstract

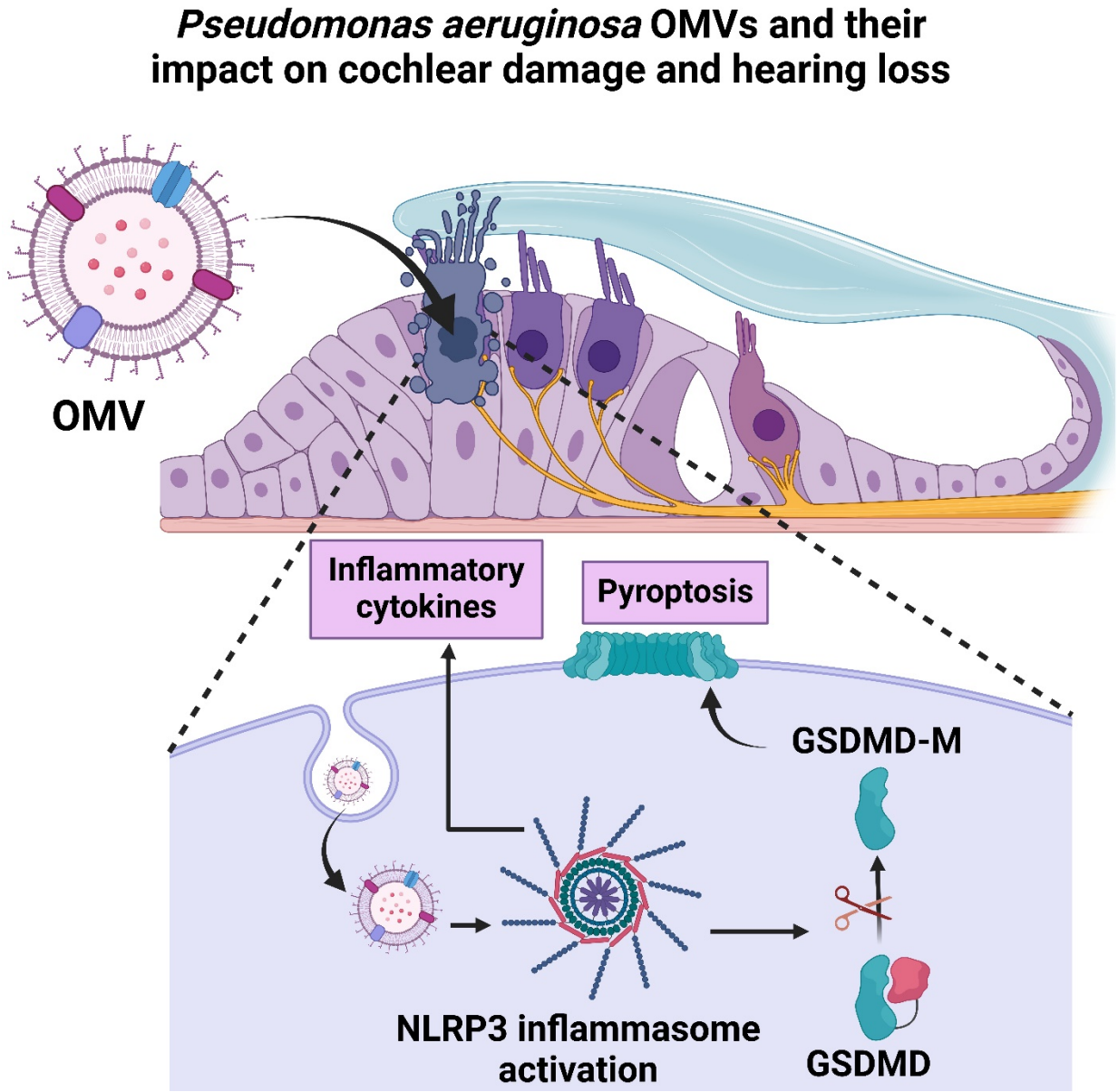

1. INTRODUCTION

Inflammasomes are multimeric protein complexes which regulate the activation of the proinflammatory cytokines interleukins-1β and 18 and inflammatory cell death called pyroptosis. Recent studies have demonstrated that NLRP3 inflammasome activation contributes to hearing loss through autoinflammatory mechanisms. Mutations in the NLRP3 gene have been implicated in both syndromic and non-syndromic forms of sensorineural hearing loss (SNHL), with some leading to the constitutive activation of this inflammasome. This dysregulation increases IL-1β release, driving local inflammation in the inner ear, which ultimately causes progressive, bilateral hearing loss.[1,2] The clinical presentation of NLRP3-related autoinflammatory disease often includes hearing loss as the main symptom. Notably, patients, particularly younger individuals, have shown positive responses to anti-IL-1 therapies, providing a promising treatment avenue for this genetic condition.[3,4]

Chronic suppurative otitis media (CSOM) is a widespread childhood infectious disease and a significant contributor to hearing impairment, particularly in low- and middle-income countries where access to healthcare may be limited. CSOM is strongly associated with SNHL, especially at higher frequencies.[5-7] The prevalence of SNHL among patients with CSOM varies significantly, ranging from 10% to 52%, likely due to differences in study populations, diagnostic criteria, and research methodologies.[5,7] Although the exact mechanisms leading to SNHL in CSOM are not fully understood, it has been shown that *Pseudomonas aeruginosa* (the most common pathogen associated with CSOM) does not invade the cochlea.[8] Additionally, cochin, cleaved to contain the LCCL domain, is secreted into the perilymph space following *the infection of Pseudomonas aeruginosa (P. aeruginosa)*. This cleaved form induces bacterial aggregation in the scala tympani, thereby preventing *P. aeruginosa* from directly damaging the hair cells.[9-11] Therefore, it is hypothesized that hair cell loss in CSOM may occur due to indirect mechanisms rather than direct bacterial invasion.

Evidence indicates that resident and infiltrating macrophages, along with NLRP3 inflammasome activation, significantly contribute to SNHL in CSOM.[8,12] However, before confirming that targeting macrophages or the NLRP3 inflammasome is a viable therapeutic strategy for SNHL in CSOM, critical gaps in our understanding need to be addressed. First, identifying the specific molecular components of *P. aeruginosa* that activate the NLRP3

inflammasome in cochlear macrophages is crucial. Furthermore, it is essential to determine the type of cell death NLRP3 activation induces in cochlear cells and how this contributes to hearing loss. Addressing these questions will be pivotal for developing targeted treatments that tackle the underlying mechanisms of SNHL in CSOM.

To address these questions, the present study investigates whether extracellular vesicles from *P. aeruginosa*, known to promote bacterial pathogenicity,[13] can trigger cochlear inflammation, activate the NLRP3 inflammasome, and lead to hair cell death. This may explain hair cell loss in CSOM as an indirect consequence of inflammation rather than a direct bacterial invasion of the cochlear. Our observations show that outer membrane vesicles (OMVs) from *P. aeruginosa* enter the cochlea and directly damage auditory hair cells. Through transcriptomic and proteomic analyses, we identified NLRP3 inflammasome-mediated pyroptosis as the critical mechanism driving hair cell damage. Notably, pharmacological inhibition of NLRP3 with MCC950 successfully prevented OMV-induced SNHL. To our knowledge, this is the first study to directly link *P. aeruginosa* OMVs with NLRP3 inflammasome activation, pyroptosis, and subsequent hair cell loss, offering a potential explanation for the reported SNHL in CSOM, despite *P. aeruginosa* not invading the cochlea.

2. MATERIAL AND METHODS

Animals and ethics approval. All animal procedures were approved by the Institutional Animal Ethics Committee (IACUC) at Shandong Provincial Hospital.

2.1. Animals

P4 and 6-8-weeks-old C57BL/6 mice (NSFC: NO.2022-110) from the animal care center of the Shandong Provincial Hospital were selected. All experimental procedures were conducted according to the guidelines outlined by the National Institutes of Health (NIH, USA) for the care and use of experimental animals. Every effort was made to minimize the number of animals used and their suffering. Try to minimize the number of animals used and reduce their suffering.

2.2. HEI-OC1 cell culture

The HEI-OC1 cell line, a widely utilized auditory cell line exhibiting characteristics of cochlear HCs, was acquired from the House Ear Institute. The cells were cultured in high-glucose DMEM (Gibco BRL, Grand Island, NY, USA) supplemented with 5% fetal bovine serum (Gibco, Grand Island, NY, USA) at 33°C in a 5% CO_2 incubator, without antibiotics.[14]

2.3. Middle ear epithelial culture

After euthanizing 6-8-weeks-old mice via inhalation anesthesia and acute decapitation, the middle ear mucosa was meticulously dissected from the superior bulla, inferior bulla, and around the tympanic orifice of the Eustachian tube under sterile conditions through the external auditory canal. The tissue fragments (1 mm^3) were then incubated in a culture medium containing penicillin and streptomycin at 4°C for at least 1 hour to minimize bacterial contamination. Subsequently, each fragment was then transferred to a 24-well tissue culture plate (Falcon) containing a culture medium composed of three parts DMEM F12 (1,056,018, Thermofsh) and one part F12, supplemented with 5% fetal bovine serum (Gibco, Grand Island, NY, USA), hydrocortisone (0.4 μg/mL, Sigma), isoproterenol (10^{-6} mol/L, Sigma), penicillin (100 U/mL, Gibco), and streptomycin (100 μg/mL, Gibco). The middle ear epithelium was then cultured in a humid environment at 37°C with 10% CO_2. On day 4, upon observation of cell growth in the culture dish, 10 ng/ml of epidermal growth factor was added to the culture medium. The culture medium was changed twice a week.[15]

2.4. Basement membrane (BM) culture and treatment

P4 C57BL/6 mice were acutely decapitated after anesthesia, and the cochlea was carefully removed. Dissect the basement membrane and lay it flat on a 10 mm thick slide pre-coated with Cell-Tak Putty containing DMEM culture medium with 10% fetal bovine serum (supplemented with 100 μM ampicillin). The BM was cultured in a complete culture medium composed of DMEM/F12, B-27 (17,504,044, Thermofsh), N-2 (17,502,048, Thermofsh), and ampicillin (a1170, Solarbio) in a CO_2 incubator (20% O_2, 5% CO_2, 75% N_2, 37°C). After 24 hours of culture, the cochlear BM tissues were cultured in a mixed medium containing 5 μg/mL OMVs for another 24 hours and then subjected to different experimental treatments.

2.5. P. aeruginosa culture

Based on our previous experimental experience,[8] *P. aeruginosa* (PAO1 strain) was inoculated on a Luria-Bertani (LB) agar plate and grown overnight at 37°C. A single colony was selected and inoculated into LB broth, then cultured at 37°C with agitation at 200 rpm for 16 hours. Subsequently, the culture was plated onto an LB agar plate and incubated for 24 hours. A single isolated colony from the second agar plate was picked and cultured in 10 mL of LB broth at 37°C, 200 rpm under aerobic conditions for 30 hours overnight, allowing the bacteria to reach a stable growth state. To generate persistent cells (PC), PAO1 was treated with 5 μg/mL ofloxacin (FLOXIN®Otic) for 5 hours, washed three times in phosphate-buffered saline (PBS) by

centrifugation at 8,000×g for 5 minutes. The pellet was resuspended in PBS. The bacterial concentration (CFU/mL) was measured by plating 100 μL of serial diluted stock solutions on LB agar plates and counting the colonies after 48 hours. A concentration of 10^{-7} CFU/mL of PC was used for subsequent experiments.

2.6. Preparation and isolation of outer membrane vesicles (OMVs)

After co-culturing PC and middle ear epithelial cells (MEEC) for 24 hours, the culture supernatant was collected and centrifuged at 8,000×g for 15 minutes. The supernatant was then passed through a 0.22 μm filter. The filtrate was concentrated using a 100 kDa centrifugal concentrator at 5,000×g for 30 minutes at 4°C. The concentrated supernatant was ultracentrifuged overnight at 100,000×g, 4°C to pellet the OMVs. The prepared OMVs were rapidly frozen in liquid nitrogen and stored at -80°C for further use. The OMVs were centrifuged at 16,000×g for 30 minutes at 4°C to remove most flagellar contamination. The sterility of the OMVs was checked by culturing 5-50 μL of the sample overnight on LB agar at 37°C.

2.7. Transmission electron microscopy

For visualization of OMVs by electron microscopy, the OMVs were diluted to 1 mg/ml in PBS, negatively stained with 2% phosphotungstic acid (pH 7.0), and directly applied to 0.5% formvar-coated 200 mesh copper grids. The samples were observed using a HITACHI transmission electron microscope (HT7800) at an accelerating voltage of 80 kV, and micrographs were taken.

2.8. Cell viability measurement

Cells were seeded at a density of 6,000 cells per well in a 96-well plate and allowed to adhere overnight. After 24 hours, the cells were treated with culture medium containing varying concentrations of OMVs (1 μg/mL, 3 μg/mL, 5 μg/mL, or 10 μg/mL) for an additional 24 hours. Subsequently, 10 μL of CCK-8 reagent (96992, Sigma-Aldrich) was added to each well and incubated for 2 hours. The absorbance at 450 nm in each well was detected for cell viability analysis, with the relative cell viability of the negative control group set as 100% viability.

2.9. OMVs fluorescent labeling

Purified vesicles were fluorescently labelled by incubation with isothiocyanate fluorescein (FITC) reagent. 1 μg FITC/μg vesicle protein was dissolved in a 100 mM NaCl/50 mM Na_2CO_3 (pH 9.2) solution and mixed for 1 hour at 37°C. HEPES washing was performed thrice (150,000×g, 30 minutes) to remove free FITC from the labelled vesicles. The sterility of the labelled vesicles was checked and, if necessary, filtered through a 0.45 μm PVDF syringe filter.

To observe the interaction of extracellular vesicles with cells or tissues, FITC-labeled vesicles (5 μg/well) were co-incubated with cells or BM at 37°C for 24 hours, and the HE-OC1 cell membrane was stained with AF 633 wheat germ agglutinin (WGA) to visualize the cell boundaries. All incubation conditions were repeated 3 times.

2.10. Enzyme-linked immunosorbent assay

Supernatants from the cochlear BMs of treated P4 mouse pups were collected. The expression of IL-1β (SEA563Mu, Life Science, Inc., Wuhan, China), IL-18 (SEA133Mu, USCN Life Science, Inc., Wuhan, China), and TNF-α (SEA064MU, USCN Life Science, Inc., Wuhan, China) was analyzed according to the manufacturer's instructions. Absorbance was measured at 450 nm using a microplate reader.

2.11. RNA sequencing analysis

Total RNA was extracted from the cochleae of mice after modelling using the AG RNA ex Pro RNA extraction kit (Catalog Number AG 21101, Accurate Biotechnology, China). The purity and concentration of RNA were assessed using the NanoDrop 2000 spectrophotometer. After the samples passed the quality test, cDNA library construction was carried out, and after the libraries passed the quality control, PE150 mode sequencing was performed using the Illumina NovaSeq6000 sequencing platform. Genes were screened using Fold Change ≥2 and FDR <0.01 as differential gene screening criteria to detect the differentially expressed genes (DEGs). The volcano and heat maps were generated using the online tool (https://hiplot. com. cn/).GO and KEGG enrichment analyses were performed using standard computational methods. The sequencing data from this study have been submitted to NCBI (https://www.ncbi.nlm.nih.gov/sra/), with the accession number.

2.12. Injection into the middle ear cavity of mice

ABR audiometry was performed on 54 C57BL/6 mice and then randomly divided into two groups, n= 7 in each group. Mice were anesthetized and positioned on a surgery platform under a microscope. The unnecessary ear skin was gently lifted to expose the tympanic membrane (TM) in the external auditory canal. Subsequently, either a 5μL solution of OMVs (5μg/mL) or a 5μL solution of OMVs+MCC950 (5μg/mg OMVs, 20μM MCC950) was injected into the unilateral middle ear cavity. In the contralateral middle ear cavity, a 5μL solution of PBS was injected as a control. The mice were maintained in a prone position for 30 minutes after injection. As described previously, mice injected with 5μL of OMVs solution exhibited III-IV

grade CSOM after 14 days. All injections were performed between 8 am and 10 am, and mice were used at different time points for all experiments. The mice were subjected to ABR audiometry 14 days later and euthanized. We selected the inner ear cochlea from three mice in each group for subsequent experiments. These experiments included paraffin sections for immunohistochemical staining, qPCR, Elisa, immunofluorescence, and RNA-seq.

2.13. Tissue sectioning and preparation

Cochlear and middle ear tissues were collected from model mice 14 days post-injection to assess potential structural abnormalities in the cochlea. These tissues were fixed overnight in pre-cooled 4% paraformaldehyde. Subsequently, the fixed cochleae underwent a series of procedures, including washing, decalcification, and embedding in paraffin. Sections of continuous 5 μm thickness were prepared, mounted on slides, and allowed to dry. The tissue sections were rehydrated and stained with hematoxylin and eosin (HE). The sections were dehydrated, cleared, and sealed with coverslips following staining. The histological characteristics were observed under a light microscope.

2.14. Measurement of auditory brainstem response (ABR)

ABR tests were conducted on the 2nd day before the injection and the 15th day after the injection, using the TDT System III (Tucker-Davis Technologies, Alachua, FL, USA). The anesthetized mice were placed in a soundproof chamber, with recording electrodes skillfully positioned on the top of the skull, reference electrodes located at the postauricular bulla, and ground electrodes placed along the midline of the back. The tests were systematically carried out at 4, 8, 12, 16, 24, and 32 kHz frequencies. Intensity levels were gradually decreased from 90 dB in 10 dB increments, and auditory thresholds were recorded at each frequency. After the tests, the mice were carefully placed on a 37°C heating pad and monitored until they fully regained consciousness.

2.15. Immunofluorescence

Cells and tissues were immersed in 4% paraformaldehyde (PFA) for 30 minutes, then permeabilized with 0.2% or 1% TritonX-100 for 30 minutes, respectively. After blocking with 1% BSA at room temperature for 1 hour, the samples were incubated with primary antibodies overnight at 4°C. The primary antibodies used in this study included Rb AF-488-anti-NLRP3 (1:50, NBP2-12446, Novus), Rb anti-Myosin7a (1:400, 25-6790, Proteus-biosciences; 38-1, DSHB), Gt anti-ASC (1:100, ab175449, Abcam), Ms anti-caspase-1 (1:500, sc-398715, Santa).

The samples were then incubated with fluorescent secondary antibodies and DAPI (Solarbio, C0060) in the dark for 1 hour. The slides were imaged using a Leica TCS SP8 fluorescence microscope.

2.16. RNA extraction and qRT-PCR

RNA was extracted from the BMs of P4 mice co-culture with OMVs (5 μg/mL) using Trizol reagent (TaKaRa, Japan). According to the manufacturer's instructions, two micrograms of total RNA were reverse-transcribed into complementary DNA (cDNA) using a Reverse Transcription kit (TaKaRa, Japan). The β-Actin gene was used as an internal housekeeping control. Measure the relative expression level of target gene mRNA. The primer sequences are listed in Table 1.

Primer Table 1

Gene	Primer sequence (5′–3′)
NLRP3	F：ATTACCCGCCCGAGAAAGG
	R：TCGCAGCAA AGATCCACACAG
ASC	F：GACAGTGCA ACTGCGAGAAG
	R：GACAGTGCA ACTGCGAGAAG
Caspase-1	F：TTCCTTCAACACCATCTACG
	R：GGTGAGCTTCTCTGGTTTTA
GSDMD	F：CGATCTCATTCCGGTGGACAG
	R：GGTTTCCAGAACCTTGAGCTTG
IL-18	F：GCAGTACGGCTTAGAGAAAA
	R：GTACATTCCACTGCCAGATT
IL-1β	F：TGCCACCTT TTGACAGTGATGA
	R：TGCCTGCCT GAAGCTCTTGT
β-Actin	F：CCACTGTCG AGTCGCGTCC
	R：GCCCACGAT GGAGGGGAATA

2.17. Cell counting

Confocal images of the immunofluorescence-stained cochlear BM were captured, and the relative length of the scale bar in the image (40 μm) was measured to calculate the total length of the cochlear epithelium. Cell quantification/0.1 mm = total number of immunopositive cells/total length of the epithelium (μm) × 100.

2.18. Statistical analysis

The results were presented as the mean ± SD of at least three independent experiments. Correlation analysis was conducted using Pearson’s correlation analysis. Statistical analysis was performed using one-way analysis of variance (ANOVA) or independent T-tests in GraphPad

Prism 10 software. The surface area of the MEEC and the number of HCs were analyzed using ImageJ software. $P < 0.05$ was considered statistically significant.

3. RESULTS

3.1. OMVs characterization

We generated OMVs by co-culturing *P. aeruginosa* (PAO1) with an established *in vitro* model of mouse middle ear epithelial cells (MEEC) (**Fig. 1A**).[16,17] Our data show that on day 3, the MEEC cells were small. By day 7, their size had significantly increased and remained stable until day 10. However, cell size decreased by day 14 (**Fig. 1B and C**). We extracted OMVs from the supernatant of a 24-hour co-culture of MEEC and *P. aeruginosa*. Transmission electron microscopy images of negatively stained OMVs showed that most were intact with a bilayer phospholipid structure, as indicated by the arrows (**Fig. 1D**). The average diameter of the OMVs was 71.9 ± 8.9 nm (**Fig. 1E**). These results confirm that we successfully produced and extracted OMVs from the co-culture.

3.2. OMVs directly damage auditory cell lines in a dose-dependent manner

We investigated whether OMVs could directly damage cochlear hair cells without macrophage involvement. OMVs were labelled with isothiocyanate fluorescein (FITC) and co-cultured with HEI-OC1 cells, while the cell membranes were stained with AF633-wheat germ agglutinin (WGA) for visualization. After 6 hours, fluorescence microscopy showed OMVs primarily at the cell membrane (**Fig. 2A**). By 12 hours, OMVs had entered the cytoplasm, and by 24 hours, they had further accumulated within the cytoplasm (**Fig. 2A**). This gradual internalization of OMVs suggests their interaction with the intracellular environment of HEI-OC1 cells.

Next, we evaluated the cytotoxic effects of OMVs on HEI-OC1 cells by treating them with 5 μg/ml OMVs for various time points (0, 6, 12, 24, and 48 hours) and with different OMVs concentrations (0, 1, 3, 5, and 10 μg/ml) for 24 hours (**Fig. 2B**). Cell viability decreased with longer incubation times, showing the highest cytotoxic effects at 48 hours (**Fig. 2C**). Additionally, cell viability declined in a concentration-dependent manner: 100% for the control, 83.3 ± 5.67% at 1 μg/ml, 75.64 ± 11.81% at 3 μg/ml, 48.63 ± 8.07% at 5 μg/ml, and 24.31 ± 6.27% at 10 μg/ml (**Fig. 2D**). These findings indicate that OMVs can enter cochlear hair cells and cause direct cell damage in both a dose- and time-dependent manner, independent of the presence of macrophages.

3.3. Direct damage to cochlear hair cells by OMVs in an ex vivo model

We used ex vivo inner ear cells to assess the effects of OMVs in a setting that closely resembles the in vivo cochlear environment. This allowed us to examine whether OMVs directly impact primary cells. We co-cultured OMVs with basilar membrane (BM) hair cells from mouse cochleae at postnatal day 4 (P4) (**Fig. 3A**). The cochlea contains inner hair cells (IHCs) and outer hair cells (OHCs), which are crucial for hearing.[18] After 24 hours, immunofluorescence staining showed OMVs accumulating in IHCs and partially entering OHCs, primarily in the middle and base regions of the cochlea (**Fig. 3B**). A schematic of the human cochlea was provided for comparison (**Fig. 3C**). Significant damage to OHCs, especially in the base (high-frequency region), was observed, including disorganization and detachment (**Fig. 3B**). Some damage was also noted in the middle turn, with a more negligible impact on IHCs (**Fig. 3B**). No significant damage was found in the apex. Hair cell survival rates were much lower in the base (36.87 ± 6.04%) compared to the middle (69.05 ± 2.33%) and apex (96.39 ± 2.72%) (**Fig. 3D**). These results confirm that OMVs directly damage auditory hair cells, particularly in the base of the cochlea, which corresponds to the high-frequency hearing region.

3.4. OMVs induce immune cell infiltration in cochlear tissue of neonatal mice

To explore the role of immune cells in OMV-induced hair cell damage, we first assessed whether OMVs increase immune cell numbers and their infiltration into the BM. We measured CD86-positive cells, a marker of M1 pro-inflammatory macrophages,[19] in the BM following OMV exposure. Our results showed a significant increase in CD86-positive cells across the cochlea's apex, middle, and base regions compared to untreated controls (**Fig. 4**). This indicates that OMVs markedly elevate M1 macrophage levels in these areas. H&E staining revealed immune cell infiltration beneath the BM in the scala tympani and along the bone lining in the scala vestibuli after OMV exposure (**Fig. S1**). Immunohistochemical analysis for CD68, a macrophage marker,[20] and myeloperoxidase (MPO), a neutrophil marker,[21] confirmed the presence of both macrophages and neutrophils. These findings suggest that OMVs induce significant immune cell migration to the vicinity of the BM. This immune cell infiltration could indirectly contribute to hair cell damage, aligning with previous studies on the impact of immune responses on sensorineural hearing loss.[22,23]

3.5. OMVs induce NLRP3 inflammasome-mediated pyroptosis in cochlear

After confirming that OMVs induce significant immune cell migration to the BM, we investigated their effects on the NLRP3 inflammasome in *ex vivo* neonatal mice cochleae at

postnatal day 4 (P4) (**Fig. 5A**). NLRP3 inflammasome activation involves the assembly of NLRP3 with ASC and pro-caspase-1, leading to the activation of caspase-1, which then cleaves IL-1β, IL-18, and gasdermin D (GSDMD). The GSDMD-N fragment forms pores in the cell membrane, causing pyroptosis and the release of IL-1β and IL-18 (**Fig. 5B**). Our results showed a significant increase in mRNA levels of NLRP3, ASC, caspase-1, IL-1β, IL-18, and GSDMD, indicating robust activation of the inflammasome pathway (**Fig. 5C**). Moreover, elevated secretion of IL-1β and IL- 18 was observed following OMV exposure (**Fig. 5D**). Confocal fluorescence imaging further confirmed the presence of NLRP3, ASC, and caspase-1 throughout the cochlea (apex, middle, and base) (**Fig. 5E**). These results demonstrate that OMVs trigger not only immune cell infiltration but also the activation of the NLRP3 inflammasome, leading to increased inflammation and pyroptosis within the cochlea.

3.6. Differential gene expression and enrichment analysis following OMV treatment

We conducted RNA sequencing (RNA-seq) analysis on cochlear tissues from mice treated with intratympanic injections of either vehicle (PBS) or OMVs (5 μg/ml) to elucidate the mechanisms by which OMVs activate the NLRP3 inflammasome. The analysis identified 2,583 differentially expressed genes (DEGs) in cochlear tissues exposed to OMVs compared to controls (**Fig. 6A**). Among these DEGs, genes linked to inflammatory responses, neuronal death, and NF-κB signalling were notably upregulated. This suggests that OMV exposure triggers a significant inflammatory response in the cochlea. Gene Ontology (GO) and KEGG pathway enrichment analyses revealed that the upregulated genes are involved in processes such as NLRP3 inflammasome assembly and related inflammatory pathways (**Fig. 6B-C**). Notably, pathways associated with NOD-like receptor signalling and NF-κB signalling were strongly enriched. These findings indicate that OMVs directly activate the NLRP3 inflammasome via these key pathways.

Specifically, the upregulation of inflammasome-related genes such as Casp1 (Caspase-1), Gsdmd (Gasdermin D), and Pycard (ASC) supports the activation of the inflammasome by OMVs (**Fig. 6D**). Caspase-1 activation is a hallmark of NLRP3 inflammasome function, leading to the maturation and secretion of pro-inflammatory cytokines IL-1β and IL-18, which were also found to be elevated in our analysis. OMVs likely initiate this response through interaction with pattern recognition receptors (PRRs). These receptors detect the microbial components on OMVs and trigger downstream signalling pathways. The NF-κB signalling

pathway was significantly enhanced following OMV exposure, as evidenced by the increased expression of Myd88, Nfkb1, Nfkb2, Rela, and Traf1 (**Fig. 6D**). Enhanced NF-κB signalling amplifies the inflammatory response by increasing cytokine production and activating further inflammasome components, creating a feedback loop that intensifies inflammation.[24] Importantly, NF-κB also connects inflammation to cell death pathways,[25] which may contribute to the observed cochlear damage. Additionally, gene set enrichment analysis (GSEA) highlighted the activation of pyroptosis, a form of programmed cell death mediated by the inflammasome.[26] The differential expression of Casp1, Gsdmd, and Ticam underscores OMV-induced pyroptosis in cochlear tissues (**Fig. 6D-G**). Pyroptosis is particularly damaging as it contributes to hair cell loss, which is strongly associated with SNHL.[27] These results provide critical insights into how OMVs contribute to hearing loss.

3.7. Differential protein expression and pathway enrichment analysis following OMV treatment

To determine if changes observed in RNA expression were reflected at the protein level, cochlear tissues were collected from mice treated with intratympanic injections of OMVs (5 μg/ml) or vehicle (PBS) and analyzed using proteomic techniques. We identified a total of 522 differentially expressed proteins (266 upregulated and 256 downregulated) with a significance cutoff of $|\log FC| > 1.5$ and $P \leq 0.05$ (**Fig. 7A**). KEGG pathway enrichment analysis revealed that these proteins were notably associated with NOD-like receptor signalling, PI3K-Akt signalling pathway, Toll-like receptor signalling, Complement and coagulation cascades (**Fig. 6B**). This finding indicates that OMVs exposure triggers robust activation of immune and inflammatory pathways in cochlear tissues.

Furthermore, gene ontology (GO) classification provided additional insights into the roles of these proteins (**Fig. 7C**). In the biological processes (BP) category, proteomic analysis revealed a significant enrichment of proteins involved in Wound Healing, Platelet Activation, Immune System Process, and Antigen Processing and Presentation. These findings suggest a robust immune response and tissue repair activation in OMV-treated cochlear tissues. In the cellular component (CC) category, proteins were predominantly localized to the extracellular region and extracellular space, indicating extracellular damage and the potential release of cellular components into the surrounding environment. In the molecular functions (MF) category, proteins associated with enzyme inhibitor activity, deaminase activity, endopeptidase inhibitor

activity, and ammonium transmembrane transporter activity were upregulated, suggesting enzyme and protease activity dysregulation.

The presence of proteins related to immune activation and tissue repair, along with extracellular protein localization, indicates that OMV-induced NLRP3 inflammasome activation likely leads to pyroptosis, an inflammatory form of cell death. This cell death mechanism involves the rupture of the cell membrane, releasing inflammatory cytokines and cellular components into the extracellular space. The upregulation of enzyme inhibitors further suggests that cochlear cells may attempt to regulate excessive protease activity, a hallmark of pyroptosis. The combined effects of immune-driven cell death, extracellular damage, and protease dysregulation likely contribute to hearing loss observed in the OMV-treated mice.

3.8. Pharmacological inhibition of NLRP3-mediated pyroptosis prevents OMV-induced hearing loss in mice

To establish a causal link between NLRP3-mediated pyroptosis and OMV-induced SNHL, we first examined whether OMV exposure leads to hearing loss in vivo. We then assessed whether inhibiting NLRP3 could prevent this pyroptosis and alleviate the associated hearing loss, aiming to explore the potential of this pathway as a therapeutic target. MCC950, a selective NLRP3 inflammasome inhibitor, was chosen based on its effectiveness in reducing pyroptosis and inflammation in various disease models.[28-31] We intratympanically injected 5 μL of vehicle control (PBS), OMVs (5 μg/ml) alone, and in combination with MCC950 (20 μM) into the middle ear cavity of C57BL/6 mice. 14 days later, we measured auditory function using auditory brainstem response (ABR) testing and subsequently sacrificed the mice to assess IHCs and OHCs loss. The results indicated that mice receiving a combination of OMVs and MCC950 maintained hearing thresholds comparable to PBS, showing no notable changes across any of the frequencies tested (**Fig. 8A**). In contrast, mice treated with OMVs alone experienced a marked elevation in hearing thresholds, particularly at higher frequencies, when compared to the PBS-treated group (**Fig. 8A**).

Next, we assessed the survival of both OHCs and IHCs 14 days after treatment, comparing groups that received PBS, OMVs alone, or OMVs combined with MCC950. IHCs remained unaffected by OMV treatment (**Fig. 8B and C**). However, significant OHC loss was observed, primarily in the basal turn (high-frequency region), with partial loss in the middle turn

(middle-frequency region) and no loss in the apical turn (low-frequency region) (**Fig. 8B and C**). This pattern of hair cell damage associated with OMV-induced NLRP3-mediated pyroptosis closely resembles the loss observed in the CSOM model inoculated with *P. aeruginosa*.[8] These findings suggest that OMVs secreted during the interaction between *P. aeruginosa* and middle ear epithelial cells facilitate the long-distance delivery of bacterial virulence factors. This process indirectly contributes to hair cell death by triggering NLRP3-mediated pyroptosis rather than through direct bacterial invasion of cochlear structures. Moreover, the absence of OHC loss in mice treated with OMVs in combination with MCC950 further supports this hypothesis (**Fig. 8B and C**). In conclusion, these findings highlight the critical role of NLRP3-mediated pyroptosis in OMV-induced hearing loss, offering compelling evidence that targeting this inflammatory pathway with inhibitors could represent a promising therapeutic strategy to prevent hair cell damage and preserve hearing in conditions such as CSOM.

4. DISCUSSION

This study aimed to uncover whether *P. aeruginosa* is a critical driver of cochlear hair cell damage and inflammation, contributing to SNHL in CSOM. While previous studies have highlighted the general cytotoxicity of OMVs from various pathogens,[32-34], their specific effect on auditory cells has yet to be discovered. Our findings fill this critical gap, revealing that *P. aeruginosa* OMVs directly damage cochlear hair cells and cause dose- and time-dependent damage. This discovery is particularly striking because the damage occurs independently of macrophage activity, pointing to a previously unrecognized mechanism by which OMVs can inflict hearing loss. This insight advances our understanding of auditory cell vulnerability in CSOM and opens new avenues for targeted therapies to protect hearing.

Our findings reveal that OMVs specifically target OHCs in the basal region of the cochlea, which plays a vital role in high-frequency hearing. This vulnerability is consistent with earlier studies showing the susceptibility of OHCs to a range of insults, such as noise exposure and ototoxic drugs.[35-38] The selective damage to OHCs suggests that OMVs may contribute to frequency-specific hearing loss, a well-recognized feature of SNHL.[39,40] In contrast, inner hair cells IHCs demonstrated resilience to OMV-induced damage, in line with their known resistance to various cochlear stressors and infections.[8,12,41-43] This differential impact underscores the distinct vulnerabilities between OHCs and IHCs when exposed to OMVs.

Additionally, our study uncovers a new layer of complexity by demonstrating that OMVs trigger robust inflammatory responses in the cochlea, marked by significant macrophage and neutrophil infiltration. This inflammation amplifies hair cell damage, reinforcing that cochlear inflammation is crucial to hearing loss. [8,12,44-49] The observed rise in CD86-positive M1 macrophages points to a pro-inflammatory environment induced by OMV exposure, consistent with earlier research that connects macrophage activity in the cochlea to CSOM-related SNHL.[8] This highlights the critical role of inflammation in worsening cochlear damage and hearing impairment.

Our study also addresses a significant gap in understanding the role of the NLRP3 inflammasome in OMV-induced SNHL. While earlier research suggested that NLRP3 inflammasome activation in cochlear macrophages could contribute to SNHL,[12] the specific triggers and types of inflammatory cell death responsible for hair cell loss remained unclear. We demonstrate that OMVs are potent triggers of NLRP3 inflammasome activation and identify pyroptosis as the specific form of cell death involved. Our RNA-sequencing and proteomic analyses confirm this mechanism and further validate the therapeutic potential of targeting the NLRP3 inflammasome pathway. The NLRP3-specific inhibitor MCC950 effectively mitigates OMV-induced hearing loss, providing compelling evidence for this approach.

Despite these significant findings, our study has some limitations. First, while we have demonstrated that *P. aeruginosa* OMVs trigger NLRP3 inflammasome activation, our research focused solely on these Gram-negative OMVs. To better understand the broader implications, it is crucial to investigate OMVs from Gram-positive bacterium pathogens which also cause CSOM, such as *Staphylococcus aureus*[49]. Additionally, our study highlights the role of OMVs in NLRP3 inflammasome activation, but further research could explore the potential of FDA-approved treatments like disulfiram, which inhibits pyroptosis by blocking gasdermin D pore formation.[50] Another promising area is investigating inhibitors that target extracellular vesicle production and release[51,52] to mitigate SNHL in our novel mouse model of CSOM.[53] These approaches could offer new therapeutic strategies for managing OMV-induced hearing loss.

5. CONCLUSION

This study highlights the pathogenic role of *P. aeruginosa* OMVs in SNHL associated with CSOM. We demonstrate that OMVs directly damage cochlear hair cells, particularly in the basal region,

leading to high-frequency hearing loss. The mechanism driving this damage is NLRP3 inflammasome-mediated pyroptotic cell death. Our findings emphasize the potential for developing therapies targeting the inflammasome or inhibiting extracellular vesicle production and release. Further studies are required to explore these therapeutic interventions.

Contributors

Junhong Zhang, Hao Zhao, Huiming Nong, Qianqian Yang, Yingxue Yuan, Jingyi Zhao, Xiru Zhang and Yanan Li performed and analyzed most of the experiments with the help of Zin Mie Mie Tun.
Junhong Zhang, Laurent A. Bekale and Zhixin Cao wrote/reviewed the manuscript.
Laurent A. Bekale and Zhixin Cao conceived and designed the study.
Zhixin Cao supervised the study.

Declaration of Interests

The authors disclose no conflicts.

Acknowledgments and Funding Declaration
We thank the National Natural Science Foundation of China Financial (NoS.82201293, 82101215), Medical and health science and technology development project of Shandong Province (No.202105010572), Youth Science Foundation Cultivation Support Program of Shandong First Medical University (No.202201-061) support provided，Qingdao Medical and Health Outstanding Young Medical Talents Training Project(2025-2027).

Data Sharing Statement

REFERENCES

1 Gregory, G. E., Munro, K. J., Couper, K. N., Pathmanaban, O. N. & Brough, D. The NLRP3 inflammasome as a target for sensorineural hearing loss. *Clin Immunol* **249**, 109287, doi:10.1016/j.clim.2023.109287 (2023).

2 Nakanishi, H. *et al.* NLRP3 mutation and cochlear autoinflammation cause syndromic and nonsyndromic hearing loss DFNA34 responsive to anakinra therapy. *Proc Natl Acad Sci U S A* **114**, E7766-e7775, doi:10.1073/pnas.1702946114 (2017).

3 Oziębło, D. *et al.* Hearing Loss as the Main Clinical Presentation in NLRP3-Associated Autoinflammatory Disease. *Front Immunol* **13**, 904632, doi:10.3389/fimmu.2022.904632 (2022).

4 Nakanishi, H. *et al.* Auditory and Vestibular Characteristics of NLRP3 Inflammasome Related Autoinflammatory Disorders: Monogenic Hearing Loss Can Be Improved by Anti-interleukin-1 Therapy. *Front Neurol* **13**, 865763, doi:10.3389/fneur.2022.865763 (2022).

5 Ali Zaidi, S. S., Pasha, H. A., Suhail, A. & Qureshi, T. A. Frequency of Sensorineural hearing loss in chronic suppurative otitis media. *J Pak Med Assoc* **66(Suppl 3)**, S42-s44 (2016).

6 Amali, A., Hosseinzadeh, N., Samadi, S., Nasiri, S. & Zebardast, J. Sensorineural hearing loss in patients with chronic suppurative otitis media: Is there a significant correlation? *Electron Physician* **9**, 3823-3827, doi:10.19082/3823 (2017).

7 Singer, A. E. A., Abdel-Naby Awad, O. G., El-Kader, R. M. A. & Mohamed, A. R. Risk factors of sensorineural hearing loss in patients with unilateral safe chronic suppurative otitis media. *Am J Otolaryngol* **39**, 88-93, doi:10.1016/j.amjoto.2018.01.002 (2018).

8 Xia, A. *et al.* Chronic suppurative otitis media causes macrophage-associated sensorineural hearing loss. *J Neuroinflammation* **19**, 224, doi:10.1186/s12974-022-02585-w (2022).

9 Rhyu, H. J., Bae, S. H., Jung, J. & Hyun, Y. M. Cochlin-cleaved LCCL is a dual-armed regulator of the innate immune response in the cochlea during inflammation. *BMB Rep* **53**, 449-452, doi:10.5483/BMBRep.2020.53.9.104 (2020).

10 Py, B. F. *et al.* Cochlin produced by follicular dendritic cells promotes antibacterial innate immunity. *Immunity* **38**, 1063-1072, doi:10.1016/j.immuni.2013.01.015 (2013).

11 Jung, J. *et al.* Cleaved Cochlin Sequesters Pseudomonas aeruginosa and Activates Innate Immunity in the Inner Ear. *Cell Host Microbe* **25**, 513-525.e516, doi:10.1016/j.chom.2019.02.001 (2019).

12 Schiel, V. *et al.* Targeting the NLRP3 inflammasome in cochlear macrophages protects against hearing loss in chronic suppurative otitis media. *J Neuroinflammation* **21**, 223, doi:10.1186/s12974-024-03212-6 (2024).

13 Villageliu, D. N. & Samuelson, D. R. The Role of Bacterial Membrane Vesicles in Human Health and Disease. *Front Microbiol* **13**, 828704, doi:10.3389/fmicb.2022.828704 (2022).

14 Zhao, H. *et al.* Cisplatin induces damage of auditory cells: Possible relation with dynamic variation in calcium homeostasis and responding channels. *Eur J Pharmacol* **914**, 174662, doi:10.1016/j.ejphar.2021.174662 (2022).

15 Nakamura, A., DeMaria, T. F., Lim, D. J. & van Blitterswijk, C. A. Primary culture of chinchilla middle ear epithelium. *Ann Otol Rhinol Laryngol* **100**, 774-782, doi:10.1177/000348949110000916 (1991).

16 Mulay, A., Akram, K., Bingle, L. & Bingle, C. D. Isolation and Culture of Primary Mouse Middle Ear Epithelial Cells. *Methods Mol Biol* **1940**, 157-168, doi:10.1007/978-1-4939-9086-3_11 (2019).

17 Mulay, A. *et al.* An in vitro model of murine middle ear epithelium. *Dis Model Mech* **9**, 1405-1417, doi:10.1242/dmm.026658 (2016).

18 Schwander, M., Kachar, B. & Müller, U. Review series: The cell biology of hearing. *J Cell Biol* **190**, 9-20, doi:10.1083/jcb.201001138 (2010).

19 Murray, P. J. *et al.* Macrophage activation and polarization: nomenclature and experimental guidelines. *Immunity* **41**, 14-20, doi:10.1016/j.immuni.2014.06.008 (2014).

20 Chistiakov, D. A., Killingsworth, M. C., Myasoedova, V. A., Orekhov, A. N. & Bobryshev, Y. V. CD68/macrosialin: not just a histochemical marker. *Lab Invest* **97**, 4-13, doi:10.1038/labinvest.2016.116 (2017).
21 Kupczyk, M., Bocheńska-Marciniak, M., Górski, P. & Kuna, P. [Myeloperoxidase (MPO) as a marker of neutrophil influx into nasal mucosa after recombinant IL-8 challenge]. *Pneumonol Alergol Pol* **70**, 544-549 (2002).
22 Woolf, N. K. & Harris, J. P. Cochlear pathophysiology associated with inner ear immune responses. *Acta Otolaryngol* **102**, 353-364, doi:10.3109/00016488609119418 (1986).
23 Liu, Y. C. & Xu, K. Macrophage-related immune responses in inner ear: a potential therapeutic target for sensorineural hearing loss. *Front Neurosci* **17**, 1339134, doi:10.3389/fnins.2023.1339134 (2023).
24 Liu, T., Zhang, L., Joo, D. & Sun, S. C. NF-κB signaling in inflammation. *Signal Transduct Target Ther* **2**, 17023-, doi:10.1038/sigtrans.2017.23 (2017).
25 Kucharczak, J., Simmons, M. J., Fan, Y. & Gélinas, C. To be, or not to be: NF-kappaB is the answer--role of Rel/NF-kappaB in the regulation of apoptosis. *Oncogene* **22**, 8961-8982, doi:10.1038/sj.onc.1207230 (2003).
26 Lu, F. *et al.* Emerging insights into molecular mechanisms underlying pyroptosis and functions of inflammasomes in diseases. *J Cell Physiol* **235**, 3207-3221, doi:10.1002/jcp.29268 (2020).
27 Gansemer, B. M., Rahman, M. T., Zhang, Z. & Green, S. H. Spiral ganglion neuron degeneration in aminoglycoside-deafened rats involves innate and adaptive immune responses not requiring complement. *Front Mol Neurosci* **17**, 1389816, doi:10.3389/fnmol.2024.1389816 (2024).
28 Dubuisson, N. *et al.* Inhibiting the inflammasome with MCC950 counteracts muscle pyroptosis and improves Duchenne muscular dystrophy. *Front Immunol* **13**, 1049076, doi:10.3389/fimmu.2022.1049076 (2022).
29 Zhang, L. *et al.* MCC950 attenuates doxorubicin-induced myocardial injury in vivo and in vitro by inhibiting NLRP3-mediated pyroptosis. *Biomed Pharmacother* **143**, 112133, doi:10.1016/j.biopha.2021.112133 (2021).
30 Zeng, W. *et al.* The selective NLRP3 inhibitor MCC950 hinders atherosclerosis development by attenuating inflammation and pyroptosis in macrophages. *Sci Rep* **11**, 19305, doi:10.1038/s41598-021-98437-3 (2021).
31 Li, S., Guo, Z. & Zhang, Z. Y. Protective effects of NLRP3 inhibitor MCC950 on sepsis-induced myocardial dysfunction. *J Biol Regul Homeost Agents* **35**, 141-150, doi:10.23812/20-662-a (2021).
32 Metruccio, M. M., Evans, D. J., Gabriel, M. M., Kadurugamuwa, J. L. & Fleiszig, S. M. Pseudomonas aeruginosa Outer Membrane Vesicles Triggered by Human Mucosal Fluid and Lysozyme Can Prime Host Tissue Surfaces for Bacterial Adhesion. *Front Microbiol* **7**, 871, doi:10.3389/fmicb.2016.00871 (2016).
33 Maldonado, R., Wei, R., Kachlany, S. C., Kazi, M. & Balashova, N. V. Cytotoxic effects of Kingella kingae outer membrane vesicles on human cells. *Microb Pathog* **51**, 22-30, doi:10.1016/j.micpath.2011.03.005 (2011).
34 Tyrer, P. C., Frizelle, F. A. & Keenan, J. I. Escherichia coli-derived outer membrane vesicles are genotoxic to human enterocyte-like cells. *Infect Agent Cancer* **9**, 2, doi:10.1186/1750-9378-9-2 (2014).
35 Ngan, E. M. & May, B. J. Relationship between the auditory brainstem response and auditory nerve thresholds in cats with hearing loss. *Hear Res* **156**, 44-52, doi:10.1016/s0378-5955(01)00264-7 (2001).
36 Escabi, C. D., Frye, M. D., Trevino, M. & Lobarinas, E. The rat animal model for noise-induced hearing loss. *J Acoust Soc Am* **146**, 3692, doi:10.1121/1.5132553 (2019).
37 Fettiplace, R. & Nam, J. H. Tonotopy in calcium homeostasis and vulnerability of cochlear hair cells. *Hear Res* **376**, 11-21, doi:10.1016/j.heares.2018.11.002 (2019).
38 Breglio, A. M. *et al.* Cisplatin is retained in the cochlea indefinitely following chemotherapy. *Nat*

Commun **8**, 1654, doi:10.1038/s41467-017-01837-1 (2017).
39 Bahmad, F., O'Malley, J., Tranebjaerg, L. & Merchant, S. N. Histopathology of nonsyndromic autosomal dominant midfrequency sensorineural hearing loss. *Otol Neurotol* **29**, 601-606, doi:10.1097/MAO.0b013e3181778245 (2008).
40 Latoche, J. R., Neely, H. R. & Noben-Trauth, K. Polygenic inheritance of sensorineural hearing loss (Snhl2, -3, and -4) and organ of Corti patterning defect in the ALR/LtJ mouse strain. *Hear Res* **275**, 150-159, doi:10.1016/j.heares.2010.12.017 (2011).
41 Amarjargal, N. *et al.* Differential vulnerability of outer and inner hair cells during and after oxygen-glucose deprivation in organotypic cultures of newborn rats. *Physiol Res* **58**, 895-902, doi:10.33549/physiolres.931466 (2009).
42 Jensen-Smith, H. C., Hallworth, R. & Nichols, M. G. Gentamicin rapidly inhibits mitochondrial metabolism in high-frequency cochlear outer hair cells. *PLoS One* **7**, e38471, doi:10.1371/journal.pone.0038471 (2012).
43 Lobarinas, E., Salvi, R. & Ding, D. Selective Inner Hair Cell Dysfunction in Chinchillas Impairs Hearing-in-Noise in the Absence of Outer Hair Cell Loss. *J Assoc Res Otolaryngol* **17**, 89-101, doi:10.1007/s10162-015-0550-8 (2016).
44 Simovic Markovic, B. *et al.* Mesenchymal Stem Cells Attenuate Cisplatin-Induced Nephrotoxicity in iNOS-Dependent Manner. *Stem Cells Int* **2017**, 1315378, doi:10.1155/2017/1315378 (2017).
45 Mwangi, M. *et al.* Interleukin-10 Attenuates Hypochlorous Acid-Mediated Cytotoxicity to HEI-OC1 Cochlear Cells. *Front Cell Neurosci* **11**, 314, doi:10.3389/fncel.2017.00314 (2017).
46 So, H. *et al.* Evidence that cisplatin-induced auditory damage is attenuated by downregulation of pro-inflammatory cytokines via Nrf2/HO-1. *J Assoc Res Otolaryngol* **9**, 290-306, doi:10.1007/s10162-008-0126-y (2008).
47 Yu, W. *et al.* Cochlear Marginal Cell Pyroptosis Is Induced by Cisplatin via NLRP3 Inflammasome Activation. *Front Immunol* **13**, 823439, doi:10.3389/fimmu.2022.823439 (2022).
48 García-Pastor, C., Blázquez-Serra, R., Bosch, R. J., Lucio Cazaña, F. J. & Fernández-Martínez, A. B. Apoptosis and cell proliferation in proximal tubular cells exposed to apoptotic bodies. Novel pathophysiological implications in cisplatin-induced renal injury. *Biochim Biophys Acta Mol Basis Dis* **1865**, 2504-2515, doi:10.1016/j.bbadis.2019.06.008 (2019).
49 Wu, L. *et al.* Oridonin alleviates kanamycin-related hearing loss by inhibiting NLRP3/caspase-1/gasdermin D-induced inflammasome activation and hair cell pyroptosis. *Mol Immunol* **149**, 66-76, doi:10.1016/j.molimm.2022.06.006 (2022).
50 Hu, J. J. *et al.* FDA-approved disulfiram inhibits pyroptosis by blocking gasdermin D pore formation. *Nat Immunol* **21**, 736-745, doi:10.1038/s41590-020-0669-6 (2020).
51 Chen, J. *et al.* Inhibitors of Bacterial Extracellular Vesicles. *Front Microbiol* **13**, 835058, doi:10.3389/fmicb.2022.835058 (2022).
52 Catalano, M. & O'Driscoll, L. Inhibiting extracellular vesicles formation and release: a review of EV inhibitors. *J Extracell Vesicles* **9**, 1703244, doi:10.1080/20013078.2019.1703244 (2020).
53 Khomtchouk, K. M. *et al.* A novel mouse model of chronic suppurative otitis media and its use in preclinical antibiotic evaluation. *Sci Adv* **6**, eabc1828, doi:10.1126/sciadv.abc1828 (2020).

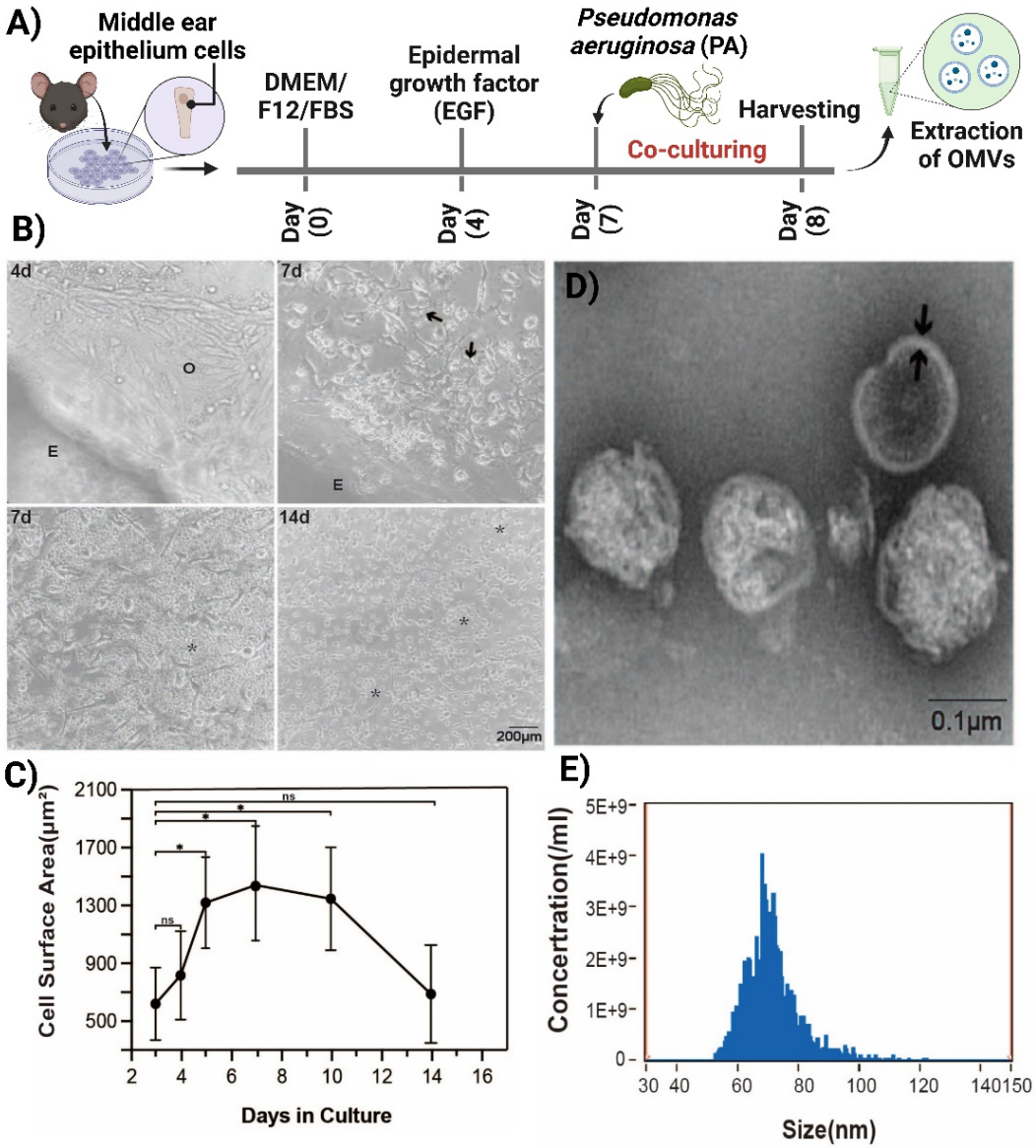

Figure 1. Characterization of OMV production and morphological changes in middle ear epithelial cells co-cultured with *P. aeruginosa*. A) Schematic illustrating the workflow for generating OMVs from *P. aeruginosa* in co-culture with middle ear epithelial cells. **B)** Morphological changes in middle ear epithelial cells over time. After 7 days in culture, the edge of the explant (*E*) shows healthy, elongated migratory hexagonal middle ear epithelial cells (MEEC), as indicated by arrows (x300). However, after 10 days, the MEEC display poor growth, transitioning to a typical polygonal shape with smaller cobblestone-like cells (x200). By day 12, the cells have reduced in size, and large multinucleated cells (*) become prominent (x200). **C)** Average cell surface area of 100 growing cells at different culture days (mean ± SD). *$p < 0.05$ compared to day 3. **D)** Transmission electron microscopy image of OMVs purified from the co- culture of *P. aeruginosa* and middle ear epithelium, showing the intact bilayer phospholipid structure of OMVs (indicated by arrows). **E)** Dynamic light scattering measurement of the size distribution of OMVs, with a diameter range of 30-150 nm.

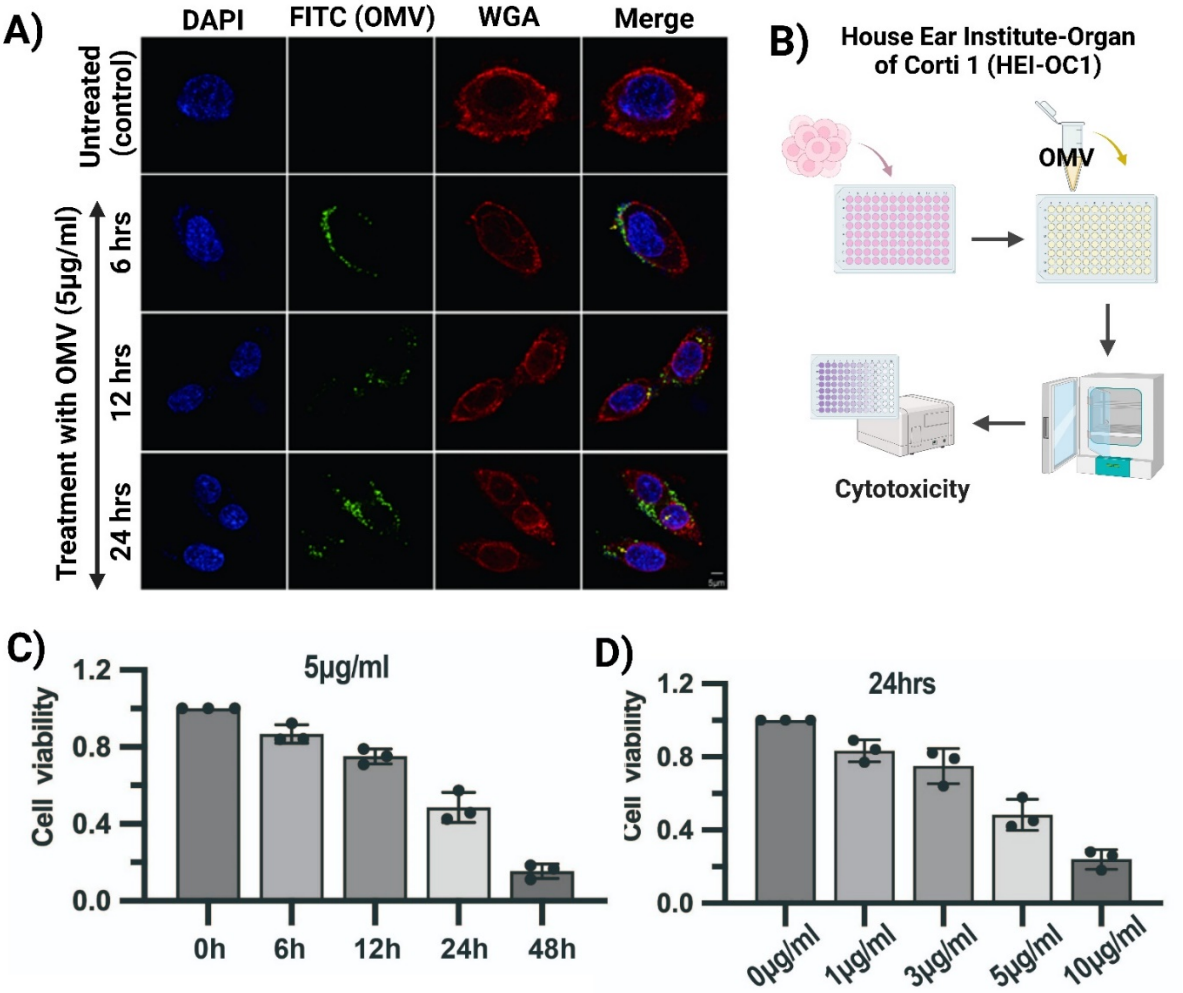

Figure 2. Evaluation of OMV Distribution and Cytotoxicity in HEI-OC1 Cells. A) The distribution of OMVs in HEI-OC1 cells was observed at various time points after 24 hours of culture. DAPI (blue fluorescence) labeled the cell nuclei, FITC (green fluorescence) marked the OMVs, and Alexa Fluor 633-wheat germ agglutinin (WGA, red fluorescence) stained the cell membranes to outline the cell boundaries. Yellow arrows highlight the locations of OMVs. Scale bar: 5 μm. **B)** A schematic shows the workflow for the CCK-8 assay used to evaluate OMV-induced cytotoxicity in HEI-OC1 cells. **C)** Cell viability of HEI-OC1 was measured over time following 24 hours of stimulation with 5 μg/ml OMVs. **D)** The cytotoxicity of OMVs was also analyzed in a concentration-dependent manner after 24 hours. All quantitative values in this figure represent the means, with error bars indicating standard deviations, from three independent experiments.

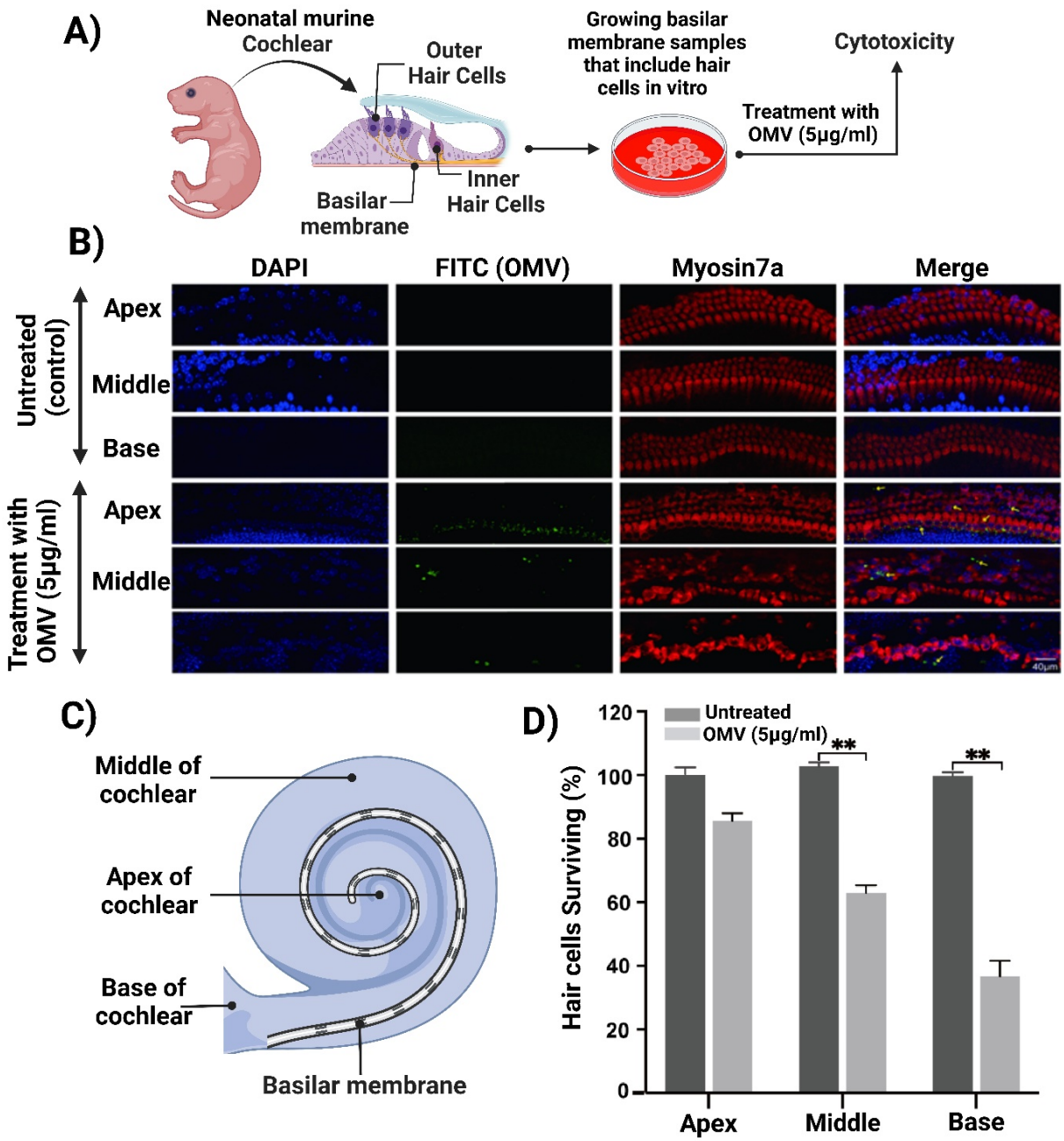

Figure 3. OMV-induced cytotoxicity and hair cell damage in *ex vivo* cochlear models. A) A schematic illustrates the workflow for assessing OMV-induced cytotoxicity in *ex vivo* cochleae from postnatal day 4 (P4) mice. **B)** Representative whole-mount cochlea sections (basal, middle, and apical turns) demonstrate OMV-induced hair cell damage. Hair cells are labelled with Myosin7a (red), and nuclei are stained with DAPI (blue). FITC (green) indicates the internalization of OMVs within cochlear hair cells, scale bar: 40 µm. A significant loss of hair cells, particularly in the basal turn, was observed following treatment with OMVs (5 µg/ml). **C)** A schematic illustrates the cochlea's localization of the basal, middle, and apical turns. **D)** Quantitative analysis of Myosin7a-positive hair cells across different groups shows a significant decrease in hair cell count (**P < 0.01). All quantitative values in this figure

represent the means, with error bars indicating standard deviations, from three independent experiments.

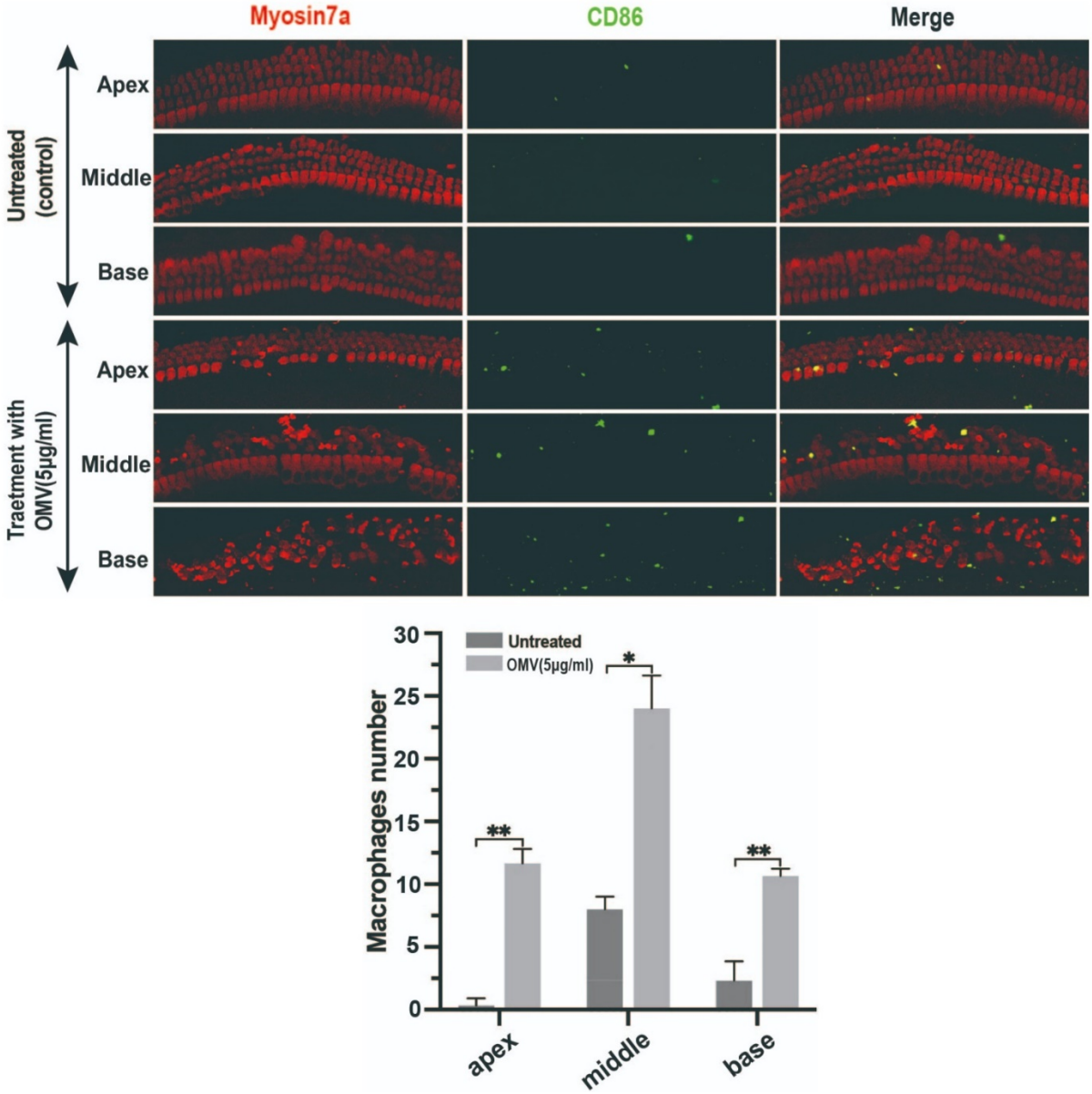

Figure 4. OMV-induced infiltration of macrophages in *ex vivo* cochlear models. Representative confocal images of cochlear whole mounts from apex, middle, and base regions showing Myosin 7a-immunolabeled hair cells (red) and macrophages are stained with CD86 (green) after treatment with OMV (5μg/ml): scale bar, 40 μm. The histogram presents a quantitative analysis of CD86-positive cells from the apex, middle, and base regions following OMV treatment, demonstrating a significant increase in the number of macrophages (**$P < 0.01$). All quantitative values in this figure represent the means, with error bars indicating standard deviations, from three independent experiments.

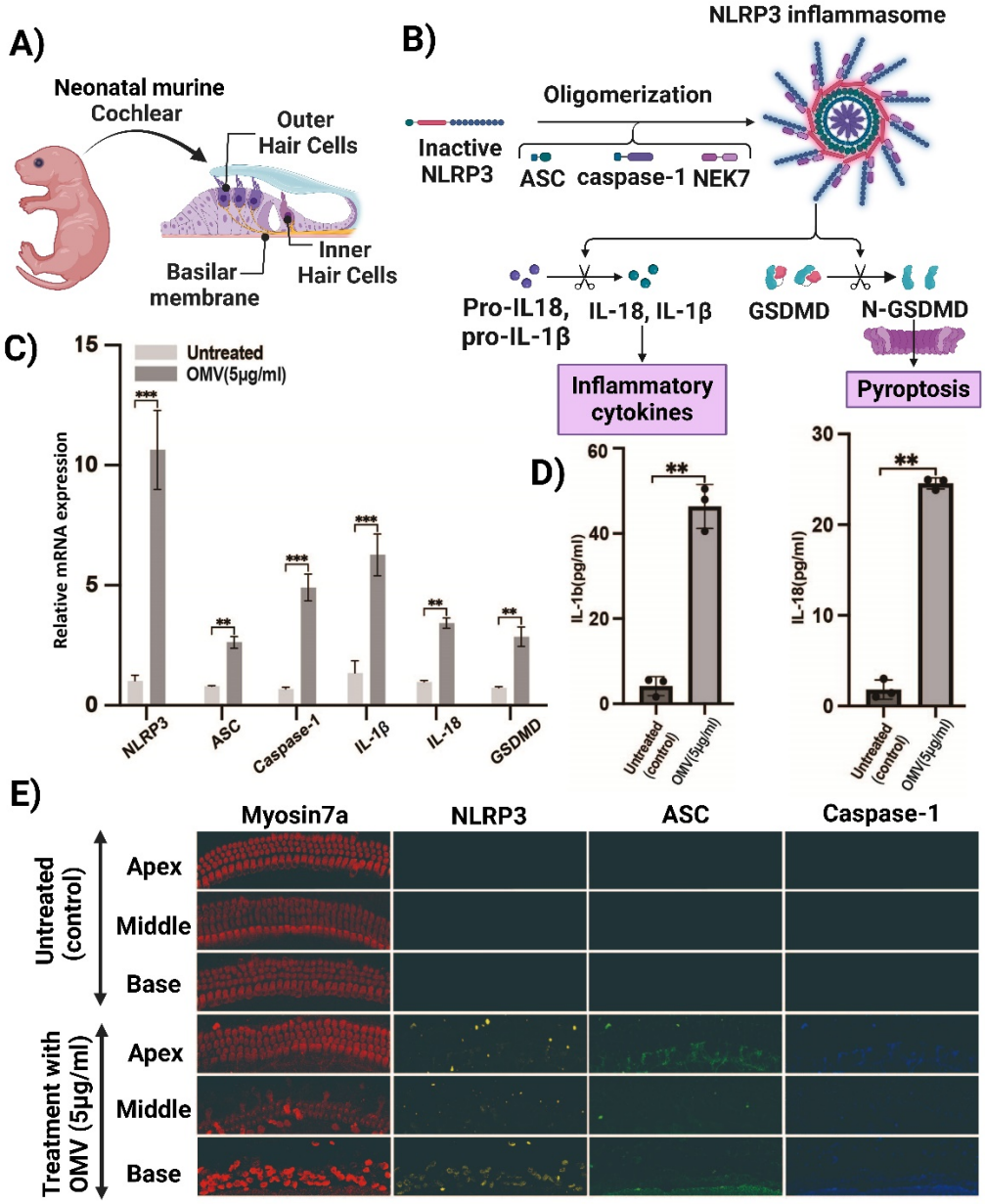

Figure 5. OMV-induced activation of NLRP3 inflammasome and pyroptosis in *ex vivo* cochlear models. A) A schematic illustrates the workflow for assessing OMV-induced NLRP3 inflammasome activation in *ex vivo* cochleae from postnatal day 4 (P4) mice. **B)** Quantitative analysis of NLRP3 inflammasome activation following OMV treatment, demonstrating a significant increase in the critical molecules in NLRP3 inflammasome-mediated pyrolysis (NLRP3, ASC, caspase-1, IL-1β, and GSDMD) in mRNA level. **C)** ELISA for IL-1β and IL-18 in medium supernatants of *ex vivo* cochleae from P4 mice treated with OMV or untreated. **D**) Representative confocal images of cochlear whole mounts from apex, middle, and base regions showing Myosin 7a-immunolabeled hair cells (red), NLRP3 inflammasome (yellow), ASC (green) and caspase-1 (bleu) after treatment with OMV (5μg/ml): scale bar, 40 μm. All quantitative values in this figure represent the means, with error bars indicating standard deviations, from three independent experiments.

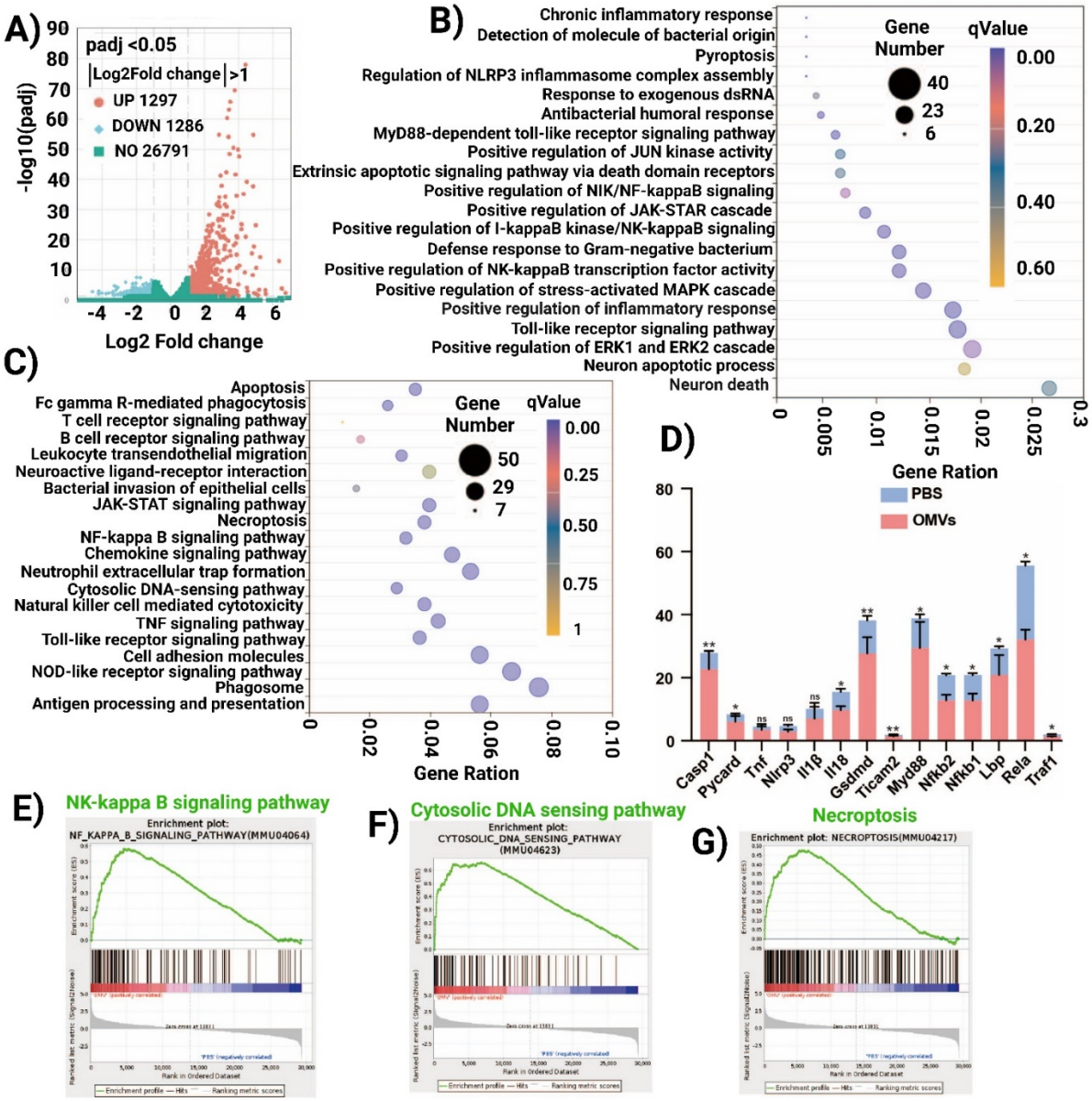

Figure 6. Differential gene expression and enrichment analysis following OMV treatment. A) Volcano plot displaying the differentially expressed genes (DEGs) following treatment with OMVs (5 µg/ml). **B-C)** Gene Ontology (GO) annotation and KEGG enrichment analysis of the DEGs to predict their potential functions, with the GO annotation results indicating that OMVs participate in several key biological processes. **D)** Differential expression analysis of the GSE 5281 dataset revealed significant changes in three genes involved in programmed cell death regulation (Casp1, Gsdmd, and Ticam), one programmed cell death-related gene (Pycard), and six NF-κB-related genes (Ticam, Myd88, Nfkb1, Nfkb2, Lbp, Rela, and Traf1). **E-F)** Gene Set Enrichment Analysis (GSEA) was performed to assess the distribution trends of genes in a ranked gene table, based on their correlation with phenotype, to determine their contribution to the phenotype.

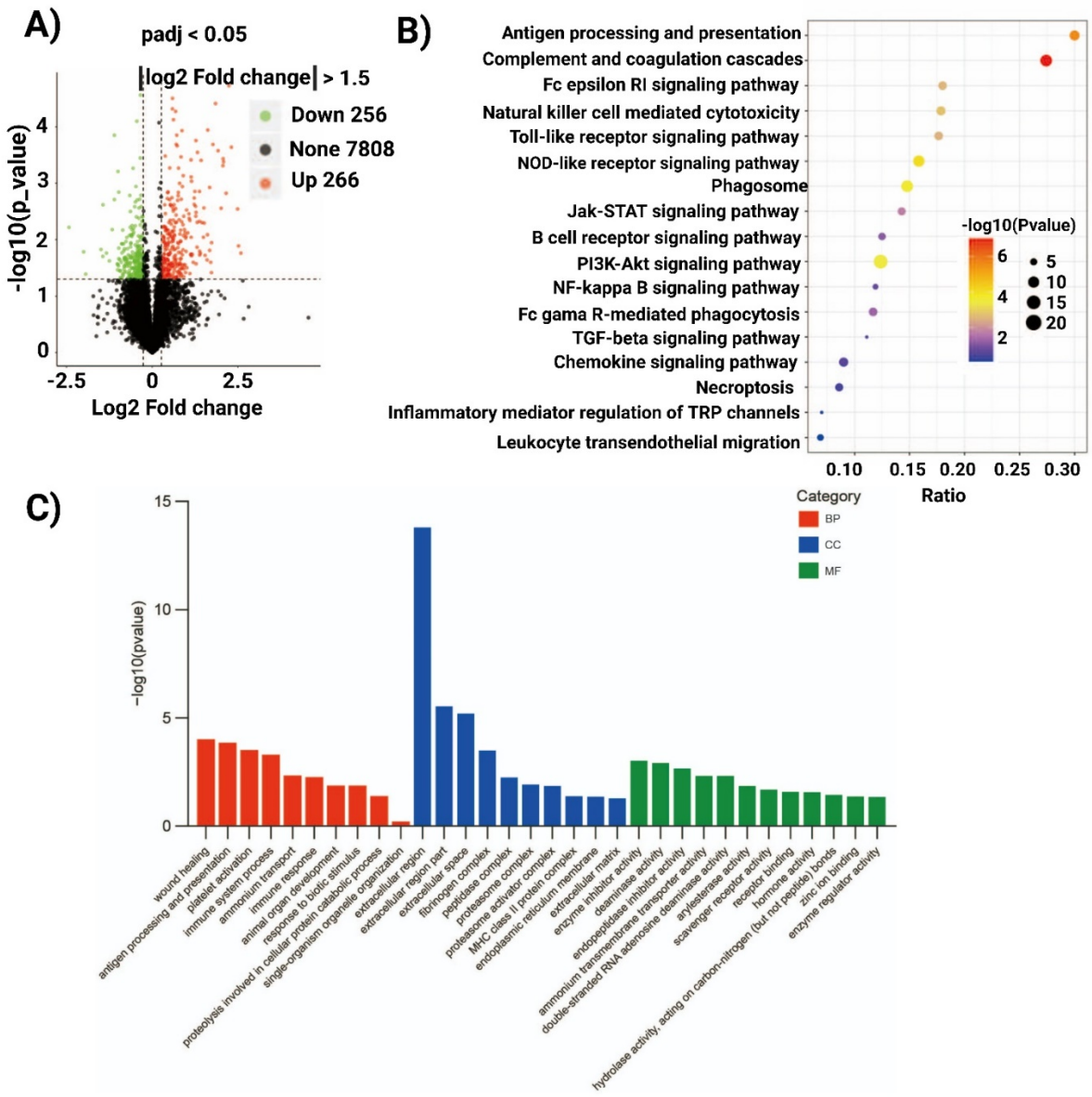

Figure 7. Differential protein expression and pathway enrichment analysis following OMV treatment. A) Volcano plot illustrating the differentially expressed proteins following treatment with OMVs (5 µg/ml). **B)** KEGG analysis results show that the differentially expressed proteins are significantly enriched in various biological pathways, including antigen processing and presentation, complement and coagulation cascades, natural killer cell-mediated cytotoxicity, Toll-like receptor signalling, NOD-like receptor signalling, phagosome formation, JAK-STAT signaling, B cell receptor signaling, NF-κB signaling, chemokine signaling, necroptosis, and leukocyte migration through endothelial cells. **C)** Summary of enriched Gene Ontology (GO) terms categorized into biological processes, cellular components, and molecular functions.

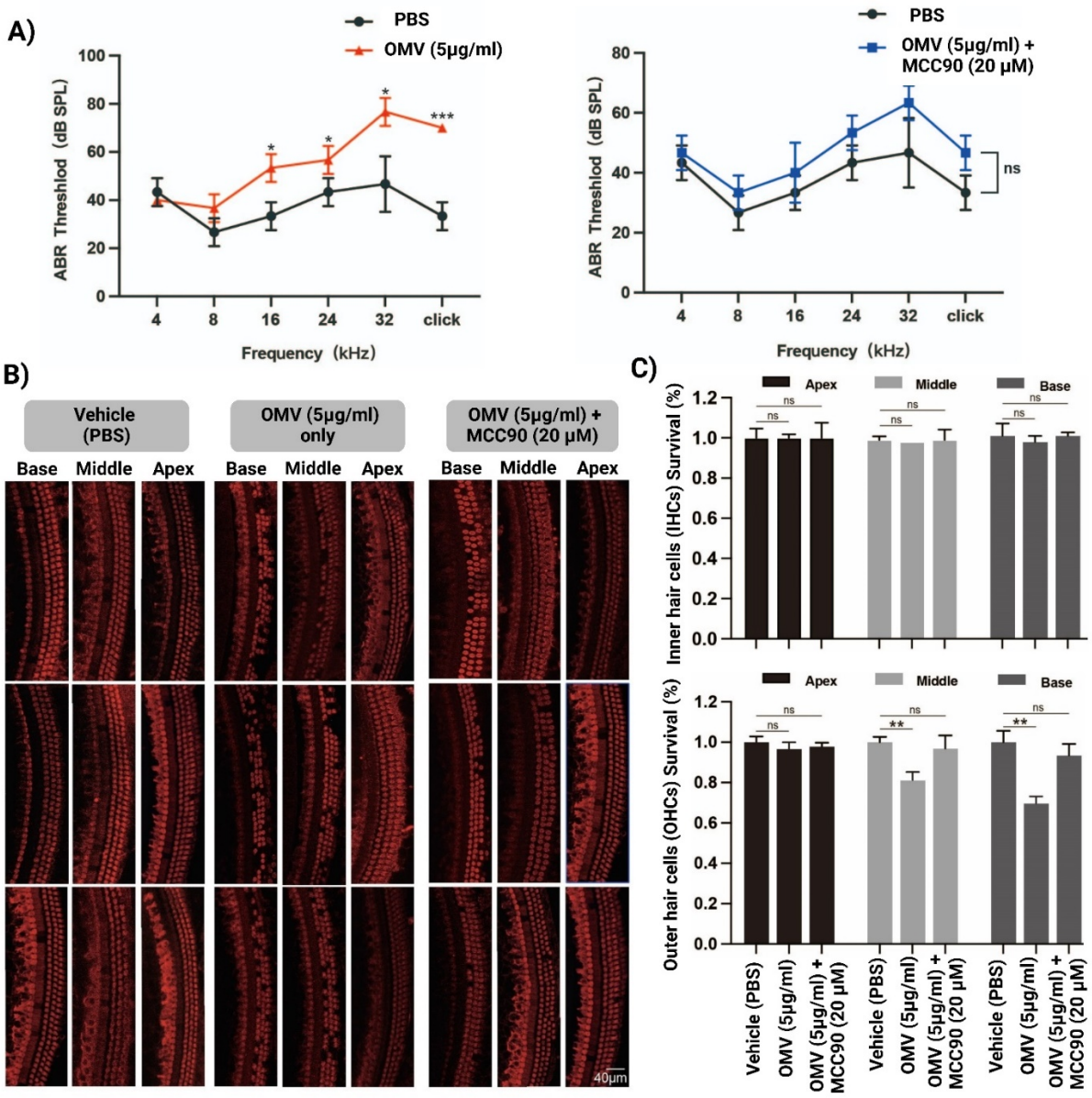

Figure 8. Pharmacological inhibition of NLRP3-mediated pyroptosis effectively prevents OMV-induced hearing loss in mice. A) Auditory brainstem response (ABR) threshold recordings were measured over 14 days following intratympanic injection of OMV (5 μg/ml) alone and in combination with MCC950 (20 μM), an NLRP3 inhibitor. These were compared to vehicle (PBS) groups, with 7 mice in each group. Mice treated with OMV alone showed impaired hearing, indicated by increased ABR thresholds. In contrast, mice treated with OMV combined with MCC950 did not exhibit a significant increase in ABR threshold. **B)** Representative confocal images of cochlear whole mounts from the apex, middle, and base regions show Myosin 7a-immunolabeled hair cells (red) following treatment with OMV alone and in combination with MCC950. Scale bar: 40 μm. **C)** After these treatments, The histogram presents a quantitative analysis of outer and inner hair cell loss from the apex, middle, and base regions, highlighting the potential of targeting the NLRP3 inflammasome to prevent OMV-induced hearing loss.

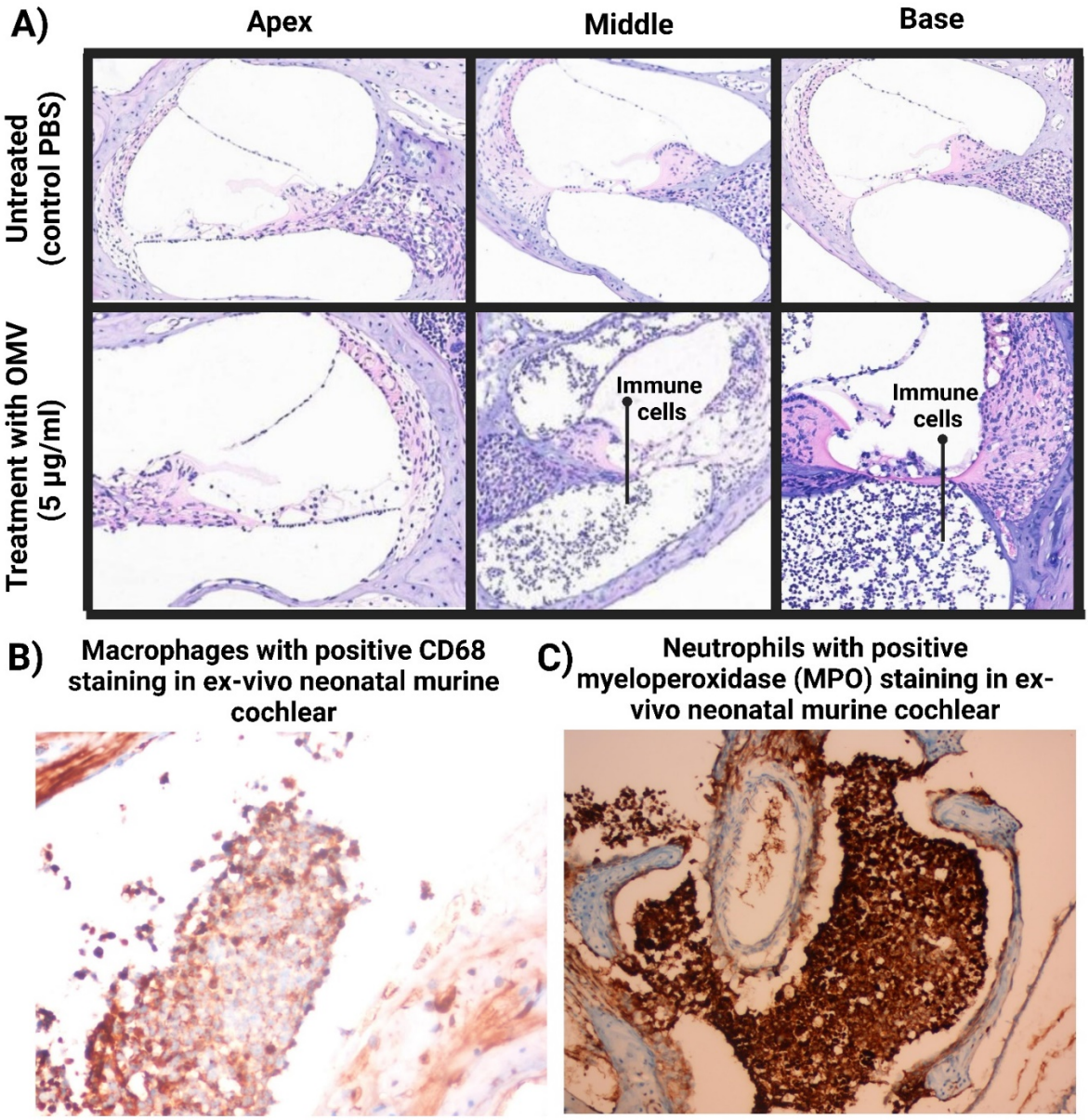

Figure S1. OMVs induce immune cell infiltration in the cochlear of neonatal mice. **A)** Representative histological sections from the inner ear (H&E staining) showing immune cell infiltration after treatment with OMV (5µg/ml). **B-C)** Immunohistochemistry staining for macrophages (CD68) and neutrophils (MPO) in the cochlear after treatment with OMV (5µg/ml).

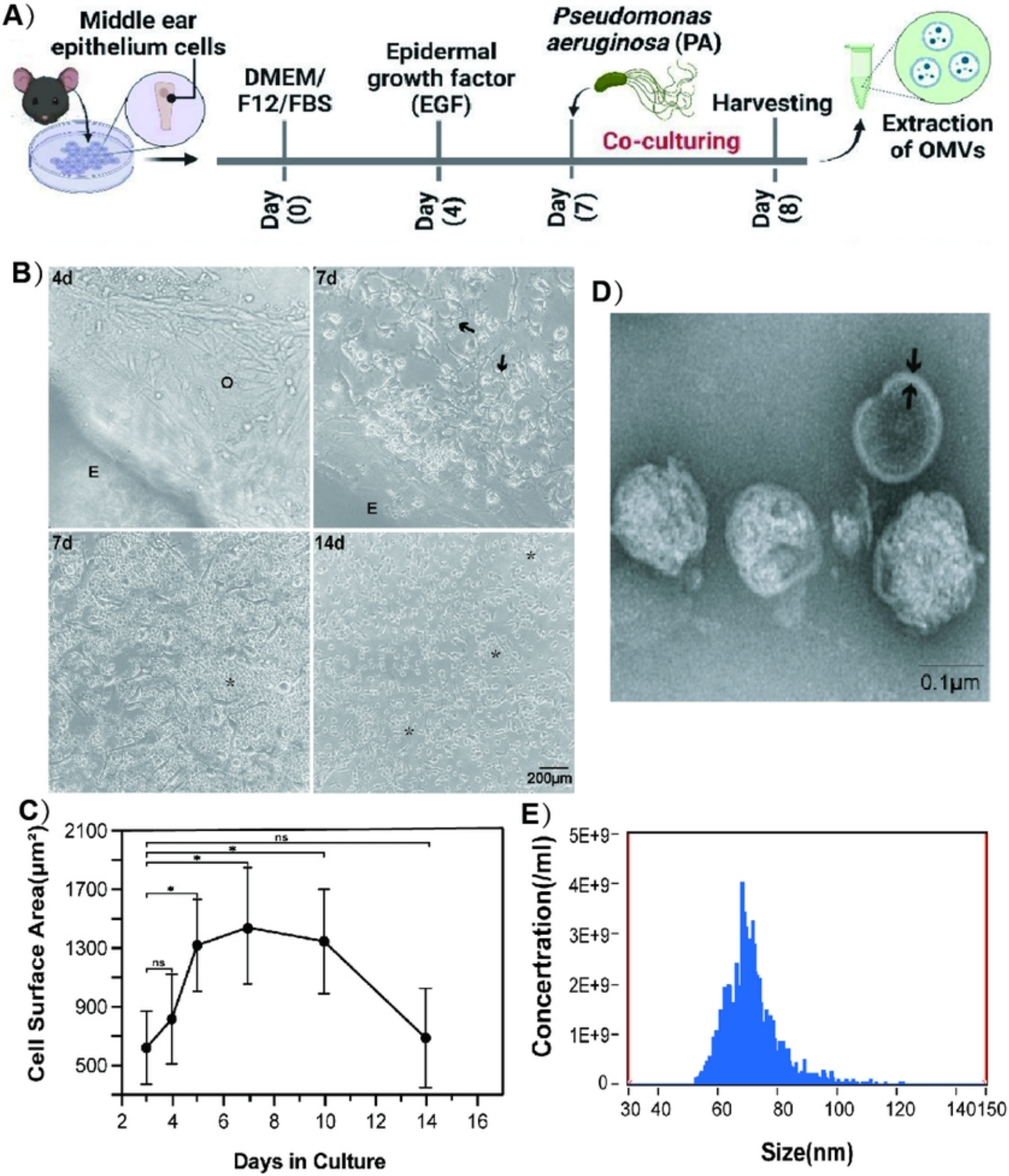
A)
Middle ear epithelium cells
DMEM/ F12/FBS
Epidermal growth factor (EGF)
Pseudomonas aeruginosa (PA)
Co-culturing
Harvesting
Extraction of OMVs
Day (0)
Day (4)
Day (7)
Day (8)
B)
4d
7d
7d
14d
O
E
E
200μm
D)
0.1μm
C)
Cell Surface Area(μm²)
2100
1700
1300
900
500
ns
*
*
*
ns
2
4
6
8
10
12
14
16
Days in Culture
E)
Concertration(/ml)
5E+9
4E+9
3E+9
2E+9
1E+9
0
30
40
60
80
100
120
140
150
Size(nm)

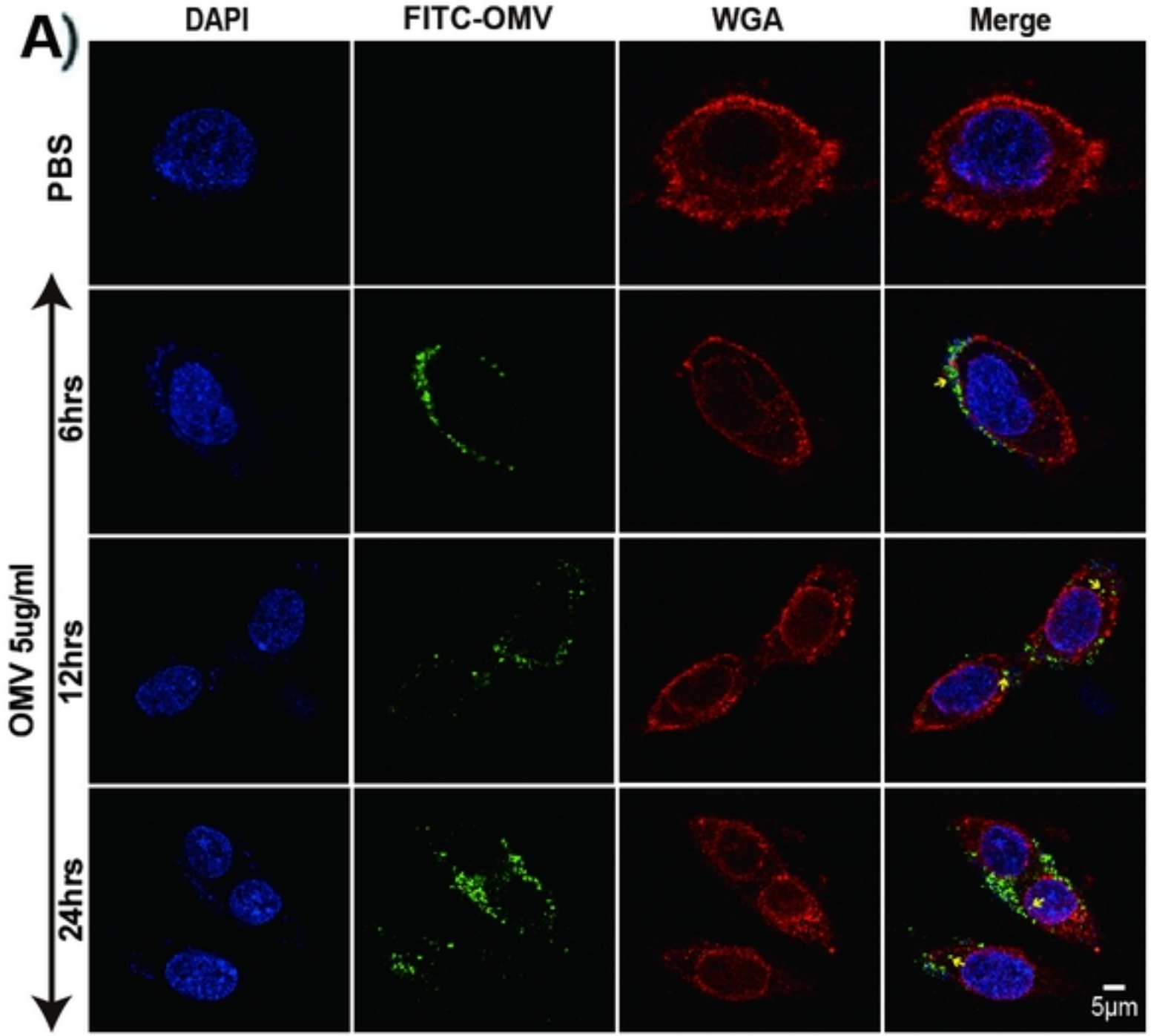
A)
DAPI
FITC-OMV
WGA
Merge
PBS
6hrs
12hrs
24hrs
OMV 5ug/ml
5μm

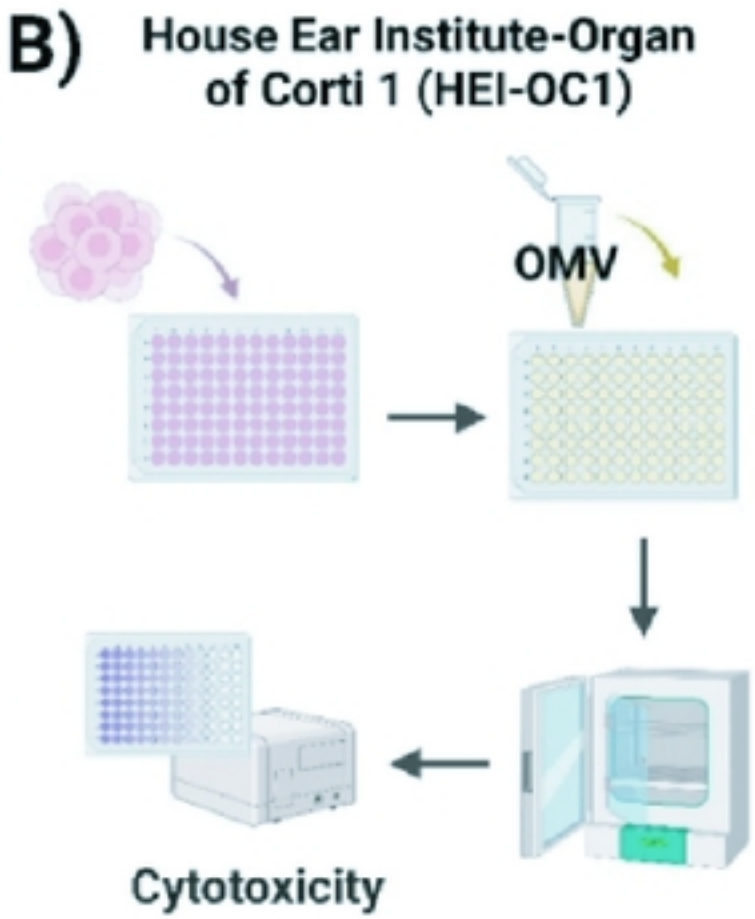
B)
House Ear Institute-Organ of Corti 1 (HEI-OC1)
OMV
Cytotoxicity

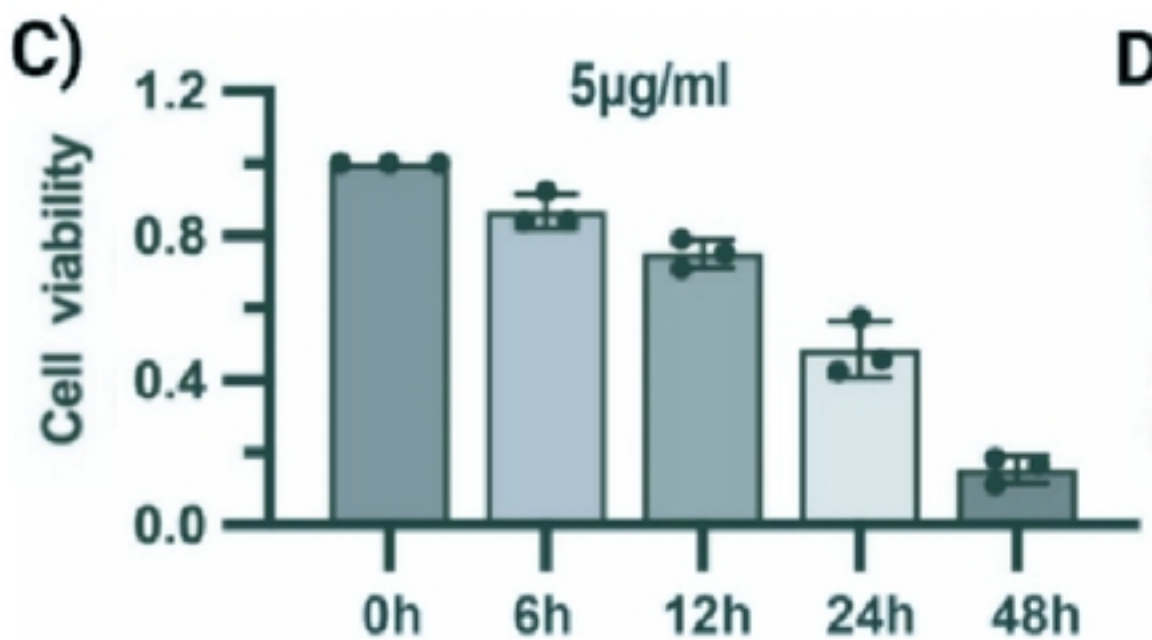
C)
5μg/ml
Cell viability
1.2
0.8
0.4
0.0
0h
6h
12h
24h
48h

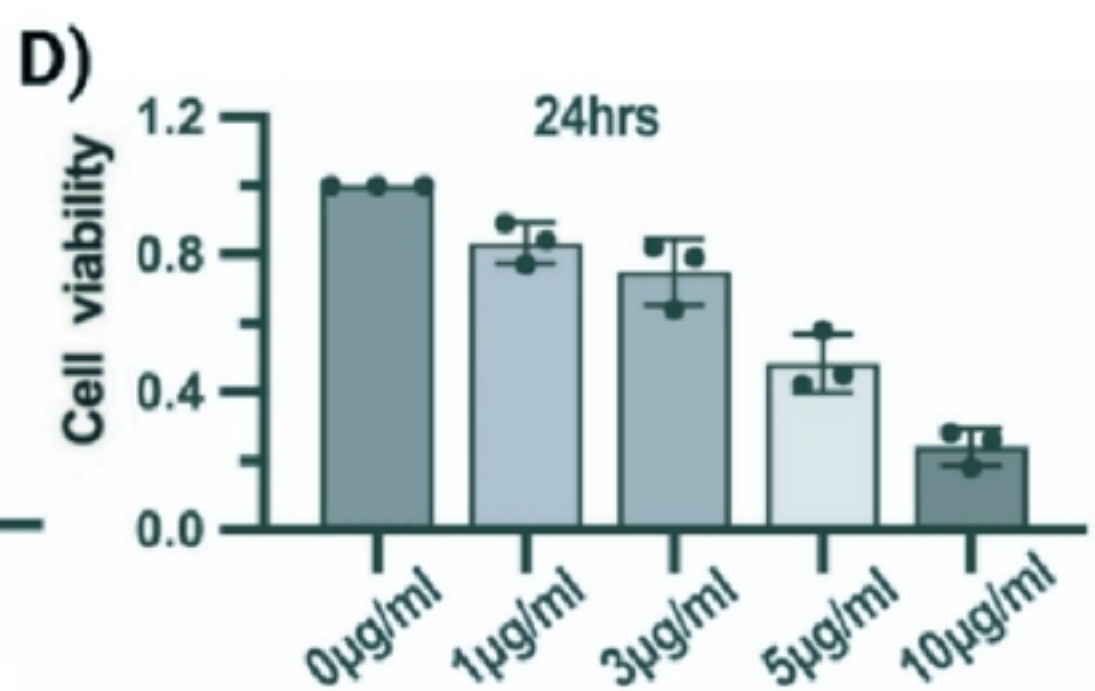
D)
24hrs
Cell viability
1.2
0.8
0.4
0.0
0μg/ml
1μg/ml
3μg/ml
5μg/ml
10μg/ml

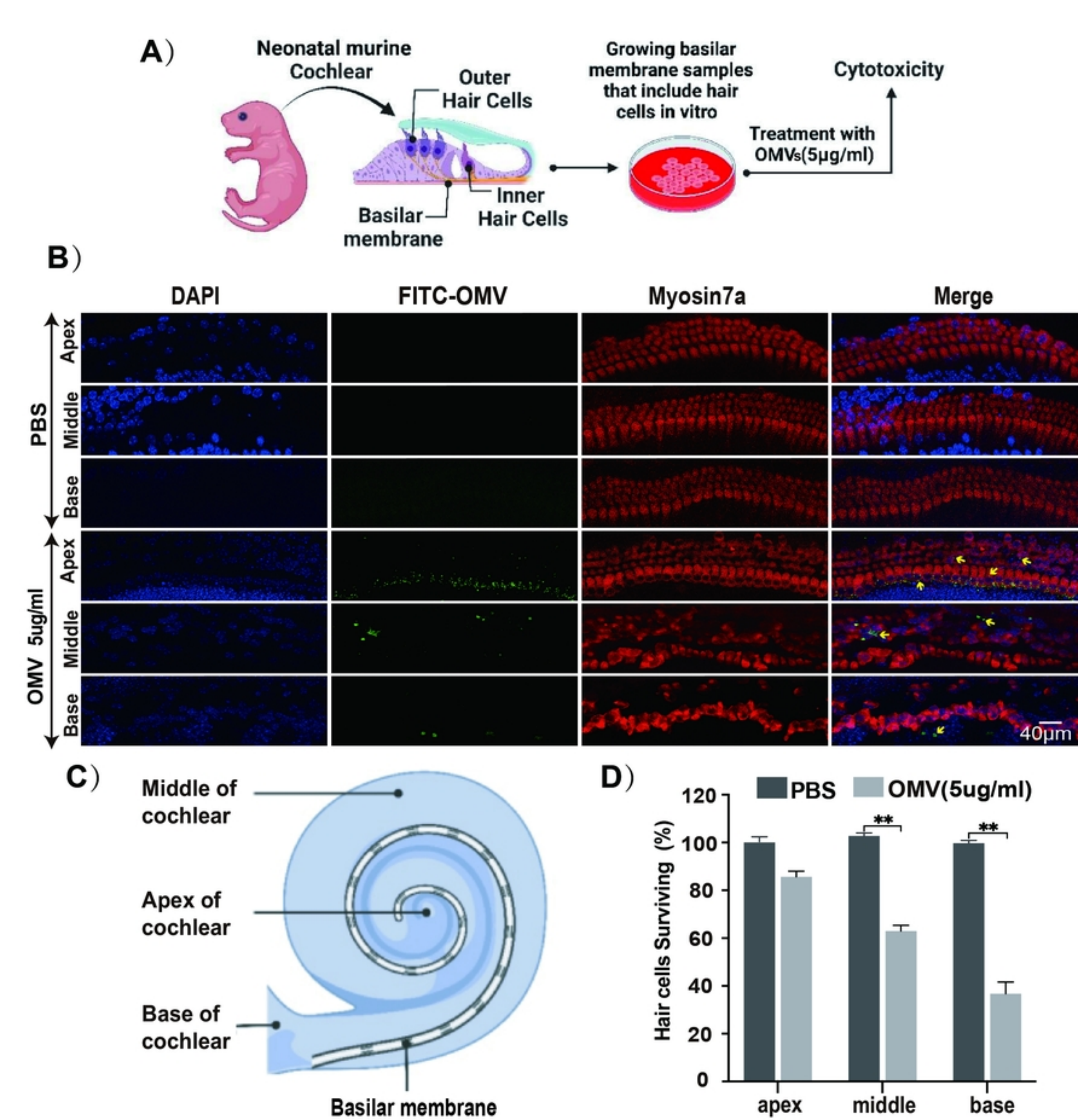
A)
Neonatal murine Cochlear
Outer Hair Cells
Inner Hair Cells
Basilar membrane
Growing basilar membrane samples that include hair cells in vitro
Treatment with OMVs(5μg/ml)
Cytotoxicity
B)
DAPI
FITC-OMV
Myosin7a
Merge
PBS
Apex
Middle
Base
OMV 5ug/ml
Apex
Middle
Base
40μm
C)
Middle of cochlear
Apex of cochlear
Base of cochlear
Basilar membrane
D)
PBS
OMV(5ug/ml)
Hair cells Surviving (%)
120
100
80
60
40
20
0
**
**
apex
middle
base

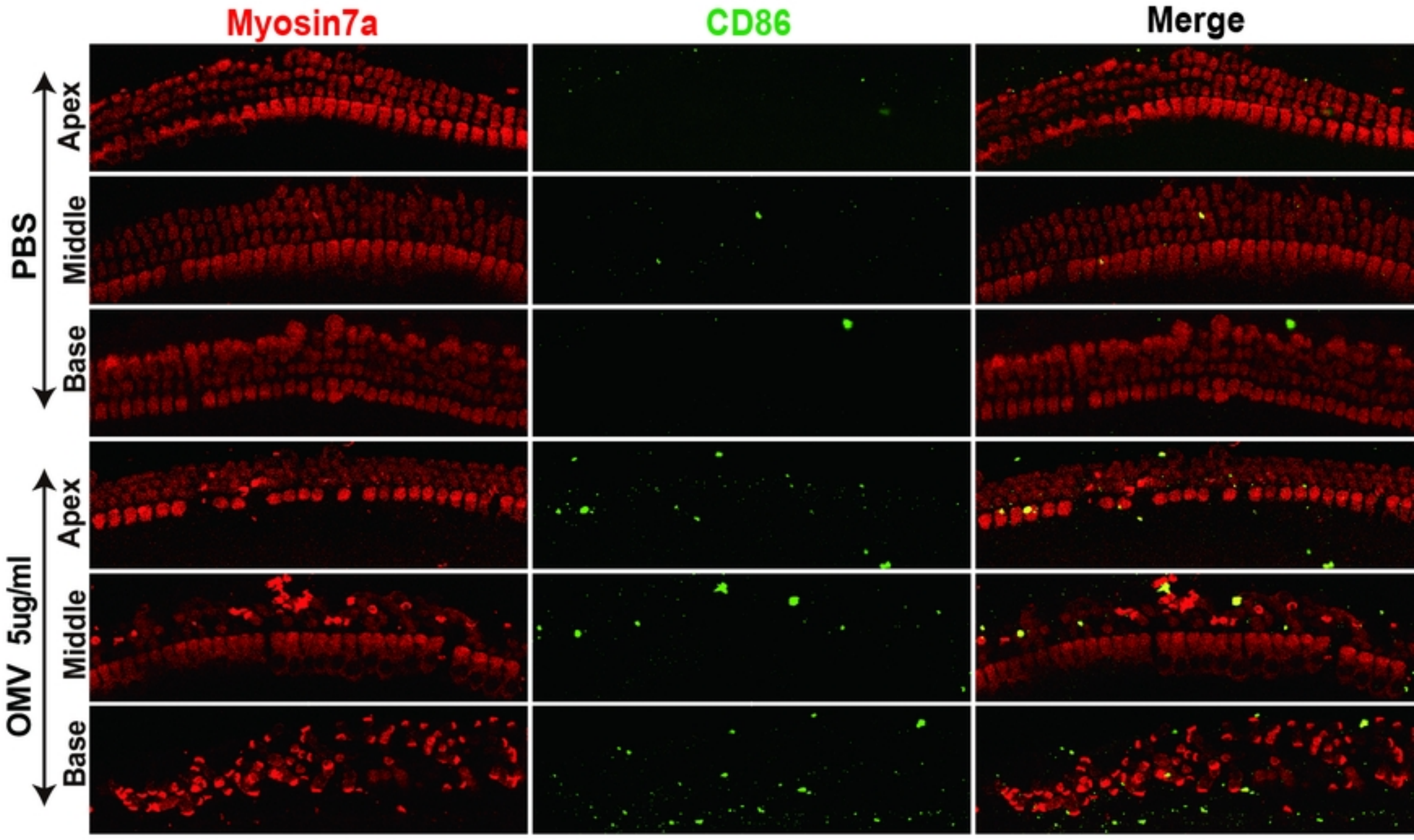
Myosin7a
CD86
Merge
PBS
Apex
Middle
Base
OMV 5ug/ml
Apex
Middle
Base

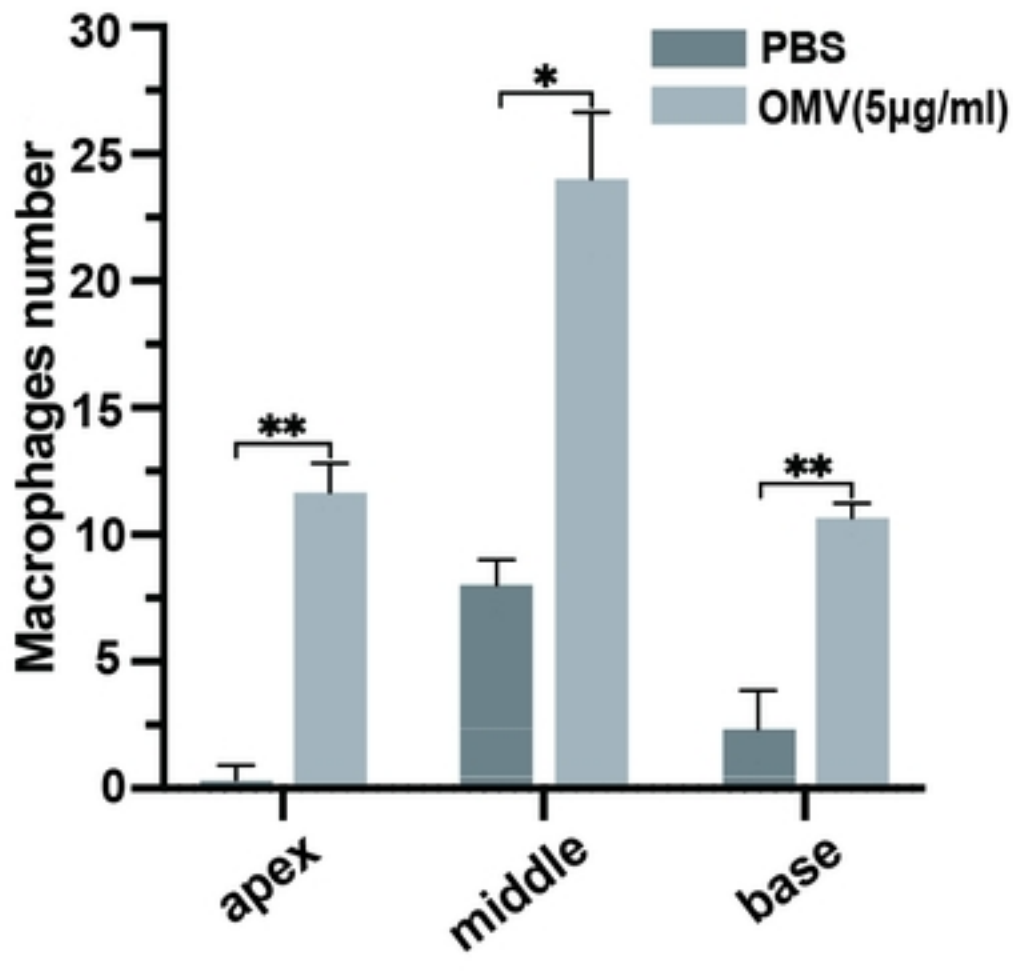
PBS
OMV(5μg/ml)
Macrophages number
30
25
20
15
10
5
0
*
**
**
apex
middle
base

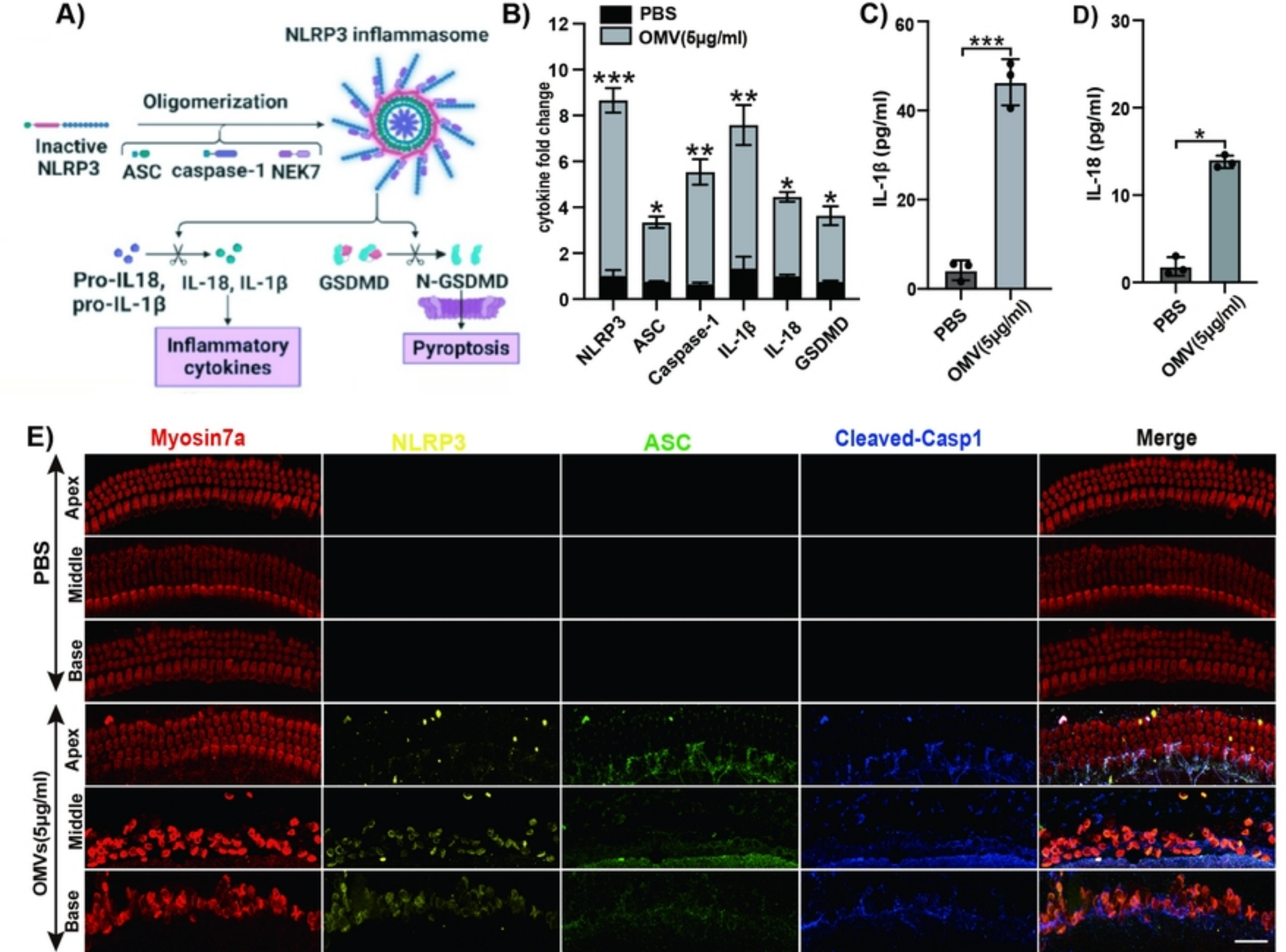
A)
NLRP3 inflammasome
Oligomerization
Inactive NLRP3
ASC
caspase-1
NEK7
Pro-IL18, pro-IL-1β
IL-18, IL-1β
GSDMD
N-GSDMD
Inflammatory cytokines
Pyroptosis
B)
PBS
OMV(5μg/ml)
cytokine fold change
NLRP3
ASC
Caspase-1
IL-1β
IL-18
GSDMD
C)
IL-1β (pg/ml)
PBS
OMV(5μg/ml)
D)
IL-18 (pg/ml)
PBS
OMV(5μg/ml)
E)
Myosin7a
NLRP3
ASC
Cleaved-Casp1
Merge
PBS
OMVs(5μg/ml)
Apex
Middle
Base

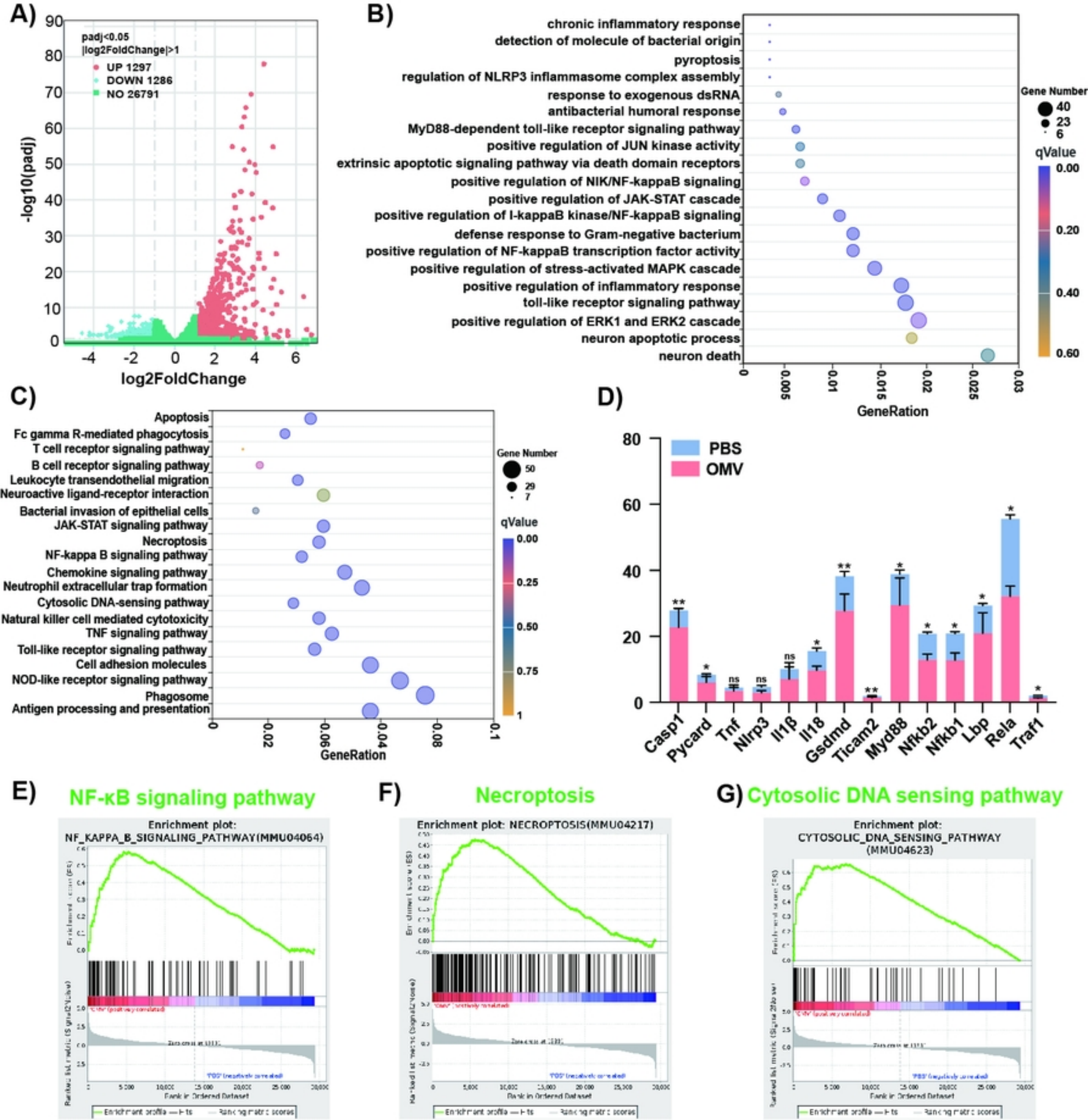
A)
padj<0.05
|log2FoldChange|>1
UP 1297
DOWN 1286
NO 26791
-log10(padj)
log2FoldChange
B)
chronic inflammatory response
detection of molecule of bacterial origin
pyroptosis
regulation of NLRP3 inflammasome complex assembly
response to exogenous dsRNA
antibacterial humoral response
MyD88-dependent toll-like receptor signaling pathway
positive regulation of JUN kinase activity
extrinsic apoptotic signaling pathway via death domain receptors
positive regulation of NIK/NF-kappaB signaling
positive regulation of JAK-STAT cascade
positive regulation of I-kappaB kinase/NF-kappaB signaling
defense response to Gram-negative bacterium
positive regulation of NF-kappaB transcription factor activity
positive regulation of stress-activated MAPK cascade
positive regulation of inflammatory response
toll-like receptor signaling pathway
positive regulation of ERK1 and ERK2 cascade
neuron apoptotic process
neuron death
GeneRation
Gene Number
qValue
C)
Apoptosis
Fc gamma R-mediated phagocytosis
T cell receptor signaling pathway
B cell receptor signaling pathway
Leukocyte transendothelial migration
Neuroactive ligand-receptor interaction
Bacterial invasion of epithelial cells
JAK-STAT signaling pathway
Necroptosis
NF-kappa B signaling pathway
Chemokine signaling pathway
Neutrophil extracellular trap formation
Cytosolic DNA-sensing pathway
Natural killer cell mediated cytotoxicity
TNF signaling pathway
Toll-like receptor signaling pathway
Cell adhesion molecules
NOD-like receptor signaling pathway
Phagosome
Antigen processing and presentation
GeneRation
Gene Number
qValue
D)
PBS
OMV
Casp1
Pycard
Tnf
Nlrp3
Il1β
Il18
Gsdmd
Ticam2
Myd88
Nfkb2
Nfkb1
Lbp
Rela
Traf1
E) NF-κB signaling pathway
Enrichment plot:
NF_KAPPA_B_SIGNALING_PATHWAY(MMU04064)
F) Necroptosis
Enrichment plot: NECROPTOSIS(MMU04217)
G) Cytosolic DNA sensing pathway
Enrichment plot:
CYTOSOLIC_DNA_SENSING_PATHWAY
(MMU04623)

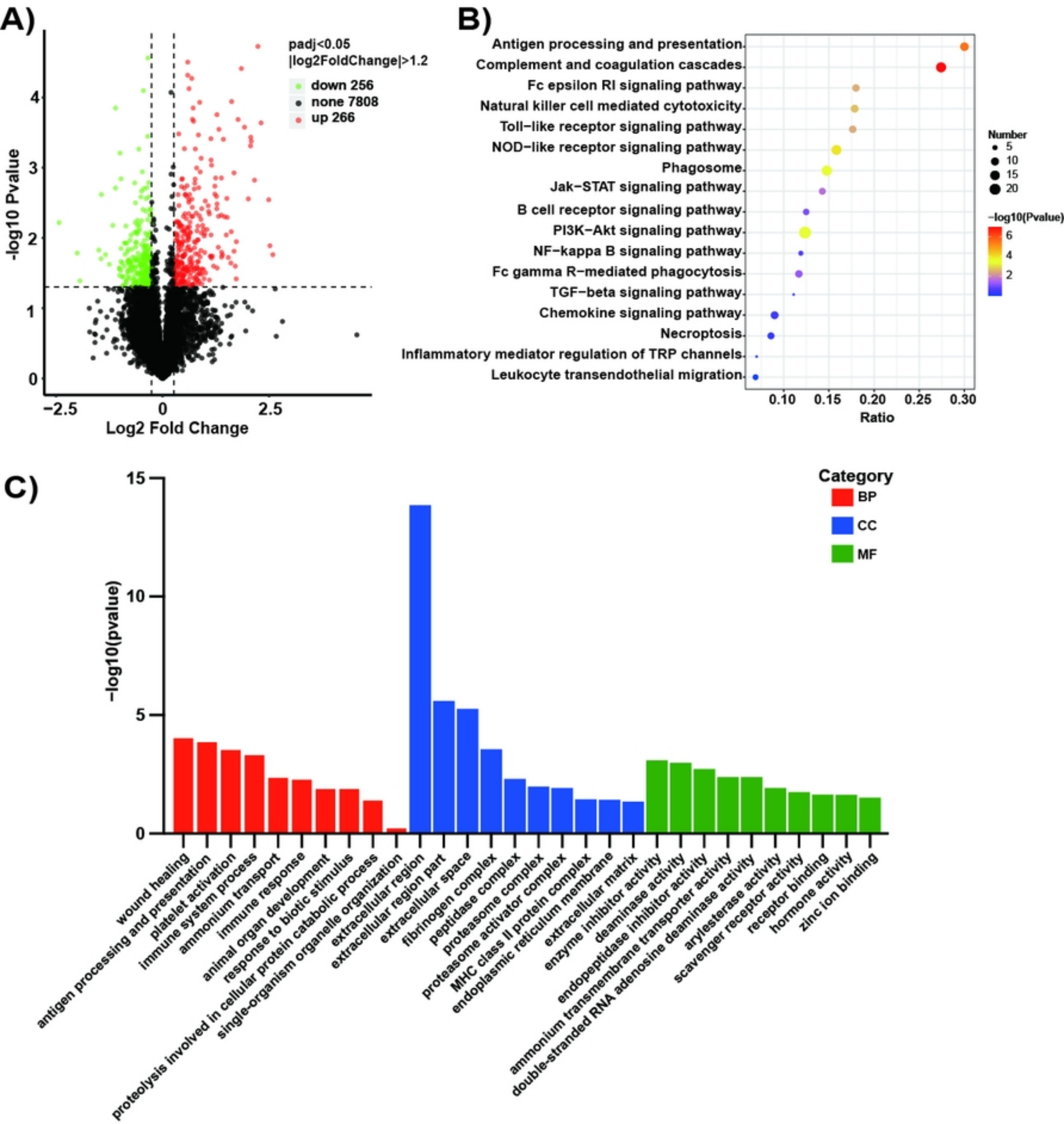
A)
padj<0.05
|log2FoldChange|>1.2
down 256
none 7808
up 266
-log10 Pvalue
Log2 Fold Change
B)
Antigen processing and presentation
Complement and coagulation cascades
Fc epsilon RI signaling pathway
Natural killer cell mediated cytotoxicity
Toll−like receptor signaling pathway
NOD−like receptor signaling pathway
Phagosome
Jak−STAT signaling pathway
B cell receptor signaling pathway
PI3K−Akt signaling pathway
NF−kappa B signaling pathway
Fc gamma R−mediated phagocytosis
TGF−beta signaling pathway
Chemokine signaling pathway
Necroptosis
Inflammatory mediator regulation of TRP channels
Leukocyte transendothelial migration
Ratio
Number
−log10(Pvalue)
C)
Category
BP
CC
MF
−log10(pvalue)
wound healing
antigen processing and presentation
platelet activation
immune system process
ammonium transport
immune response
animal organ development
response to biotic stimulus
proteolysis involved in cellular protein catabolic process
single-organism organelle organization
extracellular region
extracellular region part
extracellular space
fibrinogen complex
peptidase complex
proteasome complex
proteasome activator complex
MHC class II protein complex
endoplasmic reticulum membrane
extracellular matrix
enzyme inhibitor activity
deaminase activity
endopeptidase inhibitor activity
ammonium transmembrane transporter activity
double-stranded RNA adenosine deaminase activity
arylesterase activity
scavenger receptor activity
receptor binding
hormone activity
zinc ion binding

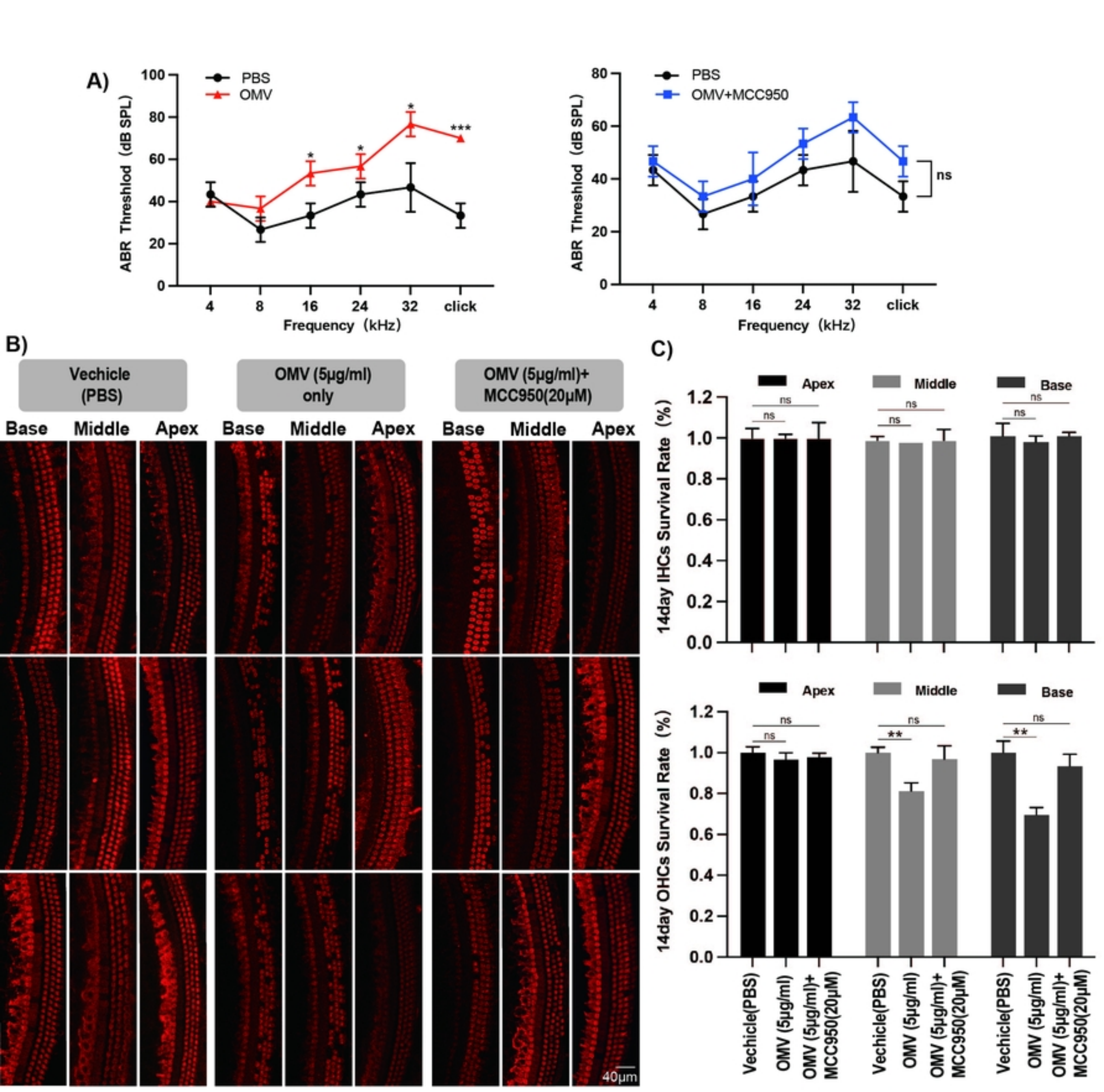
A)
PBS
OMV
ABR Threshlod (dB SPL)
Frequency (kHz)
4
8
16
24
32
click
PBS
OMV+MCC950
ns
B)
Vechicle (PBS)
OMV (5μg/ml) only
OMV (5μg/ml)+ MCC950(20μM)
Base
Middle
Apex
40μm
C)
Apex
Middle
Base
14day IHCs Survival Rate (%)
14day OHCs Survival Rate (%)
ns
**
Vechicle(PBS)
OMV (5μg/ml)
OMV (5μg/ml)+ MCC950(20μM)